AGU PUBLICATIONS

Journal of Advances in Modeling Earth Systems

RESEARCH ARTICLE
10.1002/2014MS000383

Evaluating uncertainty in convective cloud microphysics using statistical emulation

J. S. Johnson[1], Z. Cui[1], L. A. Lee[1], J. P. Gosling[2], A. M. Blyth[1,3], and K. S. Carslaw[1]

[1]Institute for Climate and Atmospheric Science, School of Earth and Environment, University of Leeds, Leeds, UK, [2]School of Mathematics, University of Leeds, Leeds, UK, [3]National Centre for Atmospheric Science, University of Leeds, Leeds, UK

Key Points:
- Processes driving uncertainty in convective cloud physics are identified
- Emulation makes comprehensive sensitivity analysis of cloud models feasible
- Aerosol effects can be smaller than many microphysical uncertainties

Correspondence to:
J. S. Johnson,
J.S.Johnson@leeds.ac.uk

Citation:
Johnson, J. S., Z. Cui, L. A. Lee, J. P. Gosling, A. M. Blyth, and K. S. Carslaw (2015), Evaluating uncertainty in convective cloud microphysics using statistical emulation, *J. Adv. Model. Earth Syst.*, *7*, 162–187, doi:10.1002/2014MS000383.

Received 2 SEP 2014
Accepted 6 JAN 2015
Accepted article online 13 JAN 2015
Published online 11 FEB 2015

Abstract The microphysical properties of convective clouds determine their radiative effects on climate, the amount and intensity of precipitation as well as dynamical features. Realistic simulation of these cloud properties presents a major challenge. In particular, because models are complex and slow to run, we have little understanding of how the considerable uncertainties in parameterized processes feed through to uncertainty in the cloud responses. Here we use statistical emulation to enable a Monte Carlo sampling of a convective cloud model to quantify the sensitivity of 12 cloud properties to aerosol concentrations and nine model parameters representing the main microphysical processes. We examine the response of liquid and ice-phase hydrometeor concentrations, precipitation, and cloud dynamics for a deep convective cloud in a continental environment. Across all cloud responses, the concentration of the Aitken and accumulation aerosol modes and the collection efficiency of droplets by graupel particles have the most influence on the uncertainty. However, except at very high aerosol concentrations, uncertainties in precipitation intensity and amount are affected more by interactions between drops and graupel than by large variations in aerosol. The uncertainties in ice crystal mass and number are controlled primarily by the shape of the crystals, ice nucleation rates, and aerosol concentrations. Overall, although aerosol particle concentrations are an important factor in deep convective clouds, uncertainties in several processes significantly affect the reliability of complex microphysical models. The results suggest that our understanding of aerosol-cloud interaction could be greatly advanced by extending the emulator approach to models of cloud systems.

1. Introduction

The interaction of aerosols with clouds is the largest uncertainty in the quantification of Earth's changing energy budget over the industrial period [*Boucher et al*., 2013]. To assess the climate impact of aerosol-cloud interaction, global model simulations of clouds and aerosols are needed, which presents substantial problems in terms of resolving the key processes in low resolution and computationally demanding climate models. However, even dedicated cloud-resolving models that include detailed aerosol and cloud microphysical processes are still subject to large uncertainty. Microphysics in clouds is complex and includes at least the activation of aerosol particles to form drops, ice formation, diffusional growth of cloud particles, and interactions between multiple types of cloud particles. The spatial scales of cloud microphysics span several orders of magnitude, and microphysical processes are interactive and can affect cloud dynamics and thermodynamics. Many cloud microphysical processes are not explicitly represented in models and therefore must be parameterized. Parameterizations of processes are based on observations, laboratory experiments and theoretical studies. However, such parameterizations are constrained by either limited observations, idealized conditions in the laboratory or theoretical assumptions, and, hence, cloud model outputs are subject to parametric uncertainty. It is important to understand the uncertainty to improve the performance of microphysical schemes for better weather forecasts and climate projection.

One approach for understanding model uncertainty is to compare different microphysics schemes within the same host dynamics model. *Morrison and Grabowski* [2007] showed that a one moment bulk scheme may produce significant errors relative to the bin model for some cases. For bulk parameterizations, a higher moment scheme generally produces better simulations [*Milbrandt and Yau*, 2006; *Morrison et al*., 2009]. *McCumber et al*. [1991] swapped parameters between a 3-class and a 2-class ice scheme and showed that the 3-class scheme is better than the 2-class scheme. Nevertheless, the most popular method is to test a single parameter or a small number of parameters in the same microphysics scheme through a one-at-a-time (OAT) test approach. The OAT test evaluates the change in the model output from some baseline case with

respect to a perturbation in a single model input. For example, *Gilmore et al*. [2004] tested various intercept parameters from an assumed size distribution conjointly with two particle densities for hail/graupel. They found that the accumulated precipitation was very sensitive to the changes in the parameters. *Adams-Selin et al*. [2013] showed the sensitivity of cloud properties to different graupel size distributions as well as the complete removal of graupel. *Dearden et al*. [2011] applied a factorial method to a single column model to investigate the sensitivity of each one in a suite of microphysics schemes. *Guo et al*. [2014] adopted a quasi-Monte Carlo sampling approach and a generalized linear model to analyze the sensitivity of properties of stratocumulus and shallow cumulus clouds to model parameters. With the intention of investigating the interactions between the parameters, *Posselt and Vukicevic* [2010] developed a Markov chain Monte Carlo algorithm to identify the uncertainty in simulating deep convective cloud with a one-dimensional model. They mapped the joint probability density function of parameters and model output state variables and found that a complex relationship exists between parameters and model output. However, the *Posselt and Vukicevic* [2010] algorithm requires 10^6 simulations in order to obtain the stationary joint probability density function for a 10 parameter analysis.

Although these previous model investigations have highlighted interesting features and dependencies as to how cloud responses change with respect to individual model parameters, very few highlight where uncertain input parameters interact and nearly all leave much of the defined parameter uncertainty space unexplored. Often this is due to the extremely large computational burden that results from the need to run the model simulator many times in order to explore the joint effects of uncertain input parameters through simultaneous parameter perturbations. With multiple uncertain inputs this can easily become impractical.

In this study, we explore the parametric uncertainty in a model of a single convective cloud, applying statistical algorithms that enable us to explore both the model sensitivity to uncertainty in individual parameters and the model sensitivity to parameter interactions at a relatively low computational cost. We balance the physical representation of the microphysical processes and the computational demand by simulating a single meteorological environment, but with bin-resolved microphysics. The simulation of a single cloud cannot account for the complex interaction between the dynamics and the microphysics that can occur in all conceivable meteorological environments. However, as we show, a detailed analysis of parametric uncertainty in cloud microphysics enables the most important parameters to be identified, which in future would allow a reduced parameter set to be applied to an ensemble of clouds formed in a range of environments.

Our approach is to use statistical emulation [*O'Hagan*, 2006] and variance-based sensitivity analysis [*Saltelli et al*., 2000], covering the full parameter space defined by the input parameter uncertainties in the calculation of our sensitivity measures. This is made possible by following the structured Bayesian statistical approach used by *Lee et al*. [2011, 2013], who examine the effects of parametric uncertainty on the simulated cloud condensation nuclei concentration within a global aerosol model. This approach takes advantage of statistical methodologies including expert elicitation [*O'Hagan et al*., 2006], statistical experiment design [*Santner et al*., 2003], Gaussian process emulation [*O'Hagan*, 2006; *Rasmussen and Williams*, 2006], and probabilistic sensitivity analysis [*Oakley and O'Hagan*, 2004; *Saltelli et al*., 2000]. The construction of a statistical emulator to represent the relationship between the set of uncertain model input parameters and the model output of interest means that we can evaluate this relationship over the full parameter uncertainty space for a very low computational cost. Therefore, this enables us to evaluate the sensitivity of the output to all of the uncertain inputs simultaneously, which allows for interaction effects to also be considered.

The Bayesian procedure begins with identifying the uncertain model input parameters and then defining the uncertainty on each one as a range outside which it is believed the true input value is very unlikely to fall. Given these uncertainty ranges, the model simulator is then run to evaluate the model outputs of interest for a designed set of targeted input combinations over the defined parameter uncertainty space, which we refer to as emulator *training runs*. Then for each chosen output (such as precipitation rate), a statistical emulator model (defined in section 3.2) is constructed based on these training runs, and once validated we can simulate from this emulator to perform a full variance-based sensitivity analysis and derive our model sensitivity measures. By exploiting the statistical tools of emulator technology and variance-based sensitivity analysis, we are able to evaluate the effects of the defined parametric uncertainty in a comprehensive way.

These methods allow us to determine how this uncertainty propagates through the model and affects the cloud responses.

The paper is structured as follows. In section 2, we describe MAC3 and the uncertain parameters, microphysical processes, and cloud responses that we wish to explore through our simulations for the formation of a deep convective cloud. In section 3, we outline the Bayesian statistical methods that we use to evaluate the sensitivity of the cloud responses to the defined parametric uncertainty. In section 4, we present the results of the sensitivity analysis, and our findings are summarized and discussed in section 5.

2. The Model of Aerosols and Chemistry in Convective Clouds, MAC3

2.1. Model Description

MAC3 is a complex cloud microphysics model that simulates the formation and development of convective clouds, given an initial set of aerosol and atmospheric conditions. MAC3 was originally developed through the work of *Reisin et al*. [1996], and has been extended and further developed by *Yin et al*. [2005]. Within the model, the cloud and aerosol microphysics are size-bin resolved. Hydrometeors (drop, ice crystal, graupel, and snow) are resolved with 34 size bins from 3 to 6400 μm for drops and 3 to 8540 μm for ice particles. Aerosol particles are resolved in 43 bins. The warm microphysical processes represented in the model include activation of CCN, diffusional growth, collision-coalescence, breakup, and evaporation. The represented cold processes are immersion freezing, deposition freezing, contact freezing, secondary ice production by the Hallett-Mossop mechanism, diffusional growth, and interaction between hydrometeors. The model is run in axisymmetric coordinates and the bin schemes are based on the method of moments by *Tzivion et al*. [1987]. MAC3 has been used to simulate and evaluate a variety of convective clouds and cloud properties, such as warm rain in shallow cumulus [*Blyth et al*., 2013], secondary ice production [*Huang et al*., 2008], aerosol effect [*Cui and Carslaw*, 2006; *Cui et al*., 2006], aerosol-cloud-precipitation interaction [*Cui et al*., 2011a], and the coupled effect of aerosol and moisture [*Cui et al*., 2011b].

The cloud simulated in this paper is a deep convective cloud in a continental environment, which has been extensively studied [e.g., *Hobbs et al*., 1985; *Respondek et al*., 1995; *Yin et al*., 2005]. *Yin et al*. [2005] compared the simulated cloud properties with observations. They found that the model reproduced the cloud reasonably well, including the base height, size of the main updraught core, updraught speed at cloud base, start time of the updraught decay, location and time of the maximum liquid-water content, concentration of droplets, first appearance of graupel, and location of the first radar echo. The initial conditions used for the thermodynamical variables here are the same as in *Yin et al*. [2005].

2.2. Choice of Uncertain Input Parameters

Eleven input parameters $\mathbf{X}=\{X_1, X_2, \ldots, X_{11}\}$ were selected to represent the main processes acting in the simulation of the deep convective cloud. A short description of each input parameter is given below, along with our assessment of the uncertainty in the values they may take, which we specify as a range of plausible values on either an absolute or a multiplicative scale. These uncertainty assessments were obtained via a small expert elicitation exercise in which information from the current literature was combined with expertise and knowledge of the capabilities of the MAC3 model itself. The inputs and uncertainty specifications are also summarized in Table 1.

The term "parameter" refers to any model quantity that can be independently perturbed to affect model output and will be used as an input to our statistical model. Some of our chosen parameters are physical quantities that can be measured in nature, such as particle density. Other parameters refer to model quantities that have no direct analogue in nature; they are model artifacts that are necessary because of model simplification. We also include aerosol particle concentrations as a parameter, even though this quantity might be considered a boundary condition on the model.

2.2.1. Graupel Density (X_1)

A graupel particle is heavily rimed and the riming rate depends on its size, mass, habit, fall speed, and the sizes and concentrations of supercooled drops and other ice particles to be collected by the graupel. Therefore, the range of graupel density is large [*Locatelli and Hobbs*, 1974; *Pruppacher and Klett*, 1997]. A bulk graupel density is commonly used in most cloud models, for example, a value of 0.4 g cm^{-3} is assumed in MAC3. However, unlike the fixed value of graupel density commonly used in models, *Milbrandt and*

Table 1. The Uncertain Model Parameters

	Parameter	Uncertainty Range	Effect
X_1	Graupel density	0.05–0.85	Absolute
X_2	Threshold between ice crystal and graupel	50–800	Absolute
X_3	Immersion freezing coefficient	0.01–100	Scaled
X_4	Deposition freezing coefficient	0.05–2	Scaled
X_5	Terminal fall speed for ice crystal	0.2–4	Scaled
X_6	Graupel aerodynamic parameter	0.5–2	Scaled
X_7	Collection efficiency of drops by graupel	0.01–10	Scaled
X_8	Collection efficiency of ice crystals by graupel	0.1–3	Scaled
X_9	Capacitance of ice crystals	0.01–10	Scaled
X_{10}	Aitken and accumulation modes of aerosol	0.01–4	Scaled
X_{11}	Coarse mode of aerosol	0.01–100	Scaled

Morrison [2013] treated the graupel density as a variable rather than a constant term and so used a range of graupel densities. In this study, we vary the graupel density over the range used in *Milbrandt and Morrison* [2013] of (0.05, 0.85) g cm^{-3}.

2.2.2. Threshold Between Ice Crystal and Graupel (X_2)

This is a threshold value at which drops with radii larger than a given size (default 100 μm) are transferred to graupel upon freezing; otherwise, they are considered as ice crystals [*Reisin et al*., 1996]. The uncertainty range for this threshold is set to be from 50 to 800 μm.

The threshold method used in this model and others imposes a fundamental problem because it necessitates artificial conversion processes. The latest scheme of *Morrison and Milbrandt* [2015] overcomes this issue by predicting particle properties and avoiding the unphysical constrained thresholds for conversion between predefined ice-phase classes.

2.2.3. Immersion Freezing (X_3)

Immersion freezing occurs when an ice nucleus is immersed within a liquid drop. Whether a drop freezes or not depends on supercooling, as well as the size, surface property, and chemical composition of the immersed nucleus. Two hypotheses have been proposed. One is stochastic and the other singular [*Murray et al*., 2012]. However, the widely used Bigg scheme for immersion freezing, also used in this paper, does not take account of the chemical composition of ice nuclei. The ice nucleating efficiency of particles varies across several orders of magnitude [*Diehl and Wurzler*, 2004]. To account for this variation in our simulations, the parameter $\overline{A}$ in the Bigg scheme [see *Cui et al*., 2006, equation (5)] is multiplied by a factor between 0.01 and 100.

2.2.4. Deposition Freezing (X_4)

Deposition freezing refers to the formation of ice in a supersaturated vapor environment, and condensation freezing is the sequence of events whereby a cloud condensation nuclei (CCN) initiates freezing of the condensate [*Vali*, 1985]. In cloud modeling, it is practically difficult to distinguish between these two freezing modes. MAC3 uses the *Meyers et al*. [1992] scheme for deposition freezing, which predicts the number concentration of ice crystals due to deposition-condensation freezing as a function of supersaturation with respect to ice. The *Meyers et al*. [1992] scheme was originally applied over the temperature range from -7°C to -20°C, from 2 to 25% ice supersaturation, and from -5% to 4.5% water supersaturation. In *Meyers et al*. [1992], the number of ice crystals is predicted via the equation:

$$N_{id} = \exp(a + bS_i),$$

where S_i is the supersaturation with respect to ice, and the constants a and b are the intercept and slope parameters for this relationship, respectively, which are derived from measurement. In our simulations, the parameter b here is multiplied by a factor between 0.05 and 2.

2.2.5. Terminal Fall Speed for Ice Crystal (X_5)

The terminal fall speed of a cloud particle is the steady velocity achieved when the drag force balances the gravitational force. There is little uncertainty about the terminal fall speeds of liquid drops. However, the uncertainty in terminal fall speeds of ice particles is large. This uncertainty could originate from the relationship between the size and mass of an ice particle because of the irregular shape. Alternatively, it may also come from the drag force since the theory available for calculating drag force is restricted to semiempirical

methods, and the drag coefficient is extremely difficult to determine accurately [*Pruppacher and Klett*, 1997]. Fall speed differences between different schemes can be very large [*Mitchell and Heymsfield*, 2005]. The terminal fall speeds (in cm s^{-1}) for ice particles in MAC3 are obtained by the *Böhm* [1989] formulation which is a function of the particle mass, the kinematic viscosity, the Reynolds number, and the ratio of the effective projected area to the circumscribed area of the particle. The terminal fall speed for ice crystal is multiplied by a factor between 0.2 and 4.

2.2.6. Graupel Aerodynamic Parameter Affecting Terminal Fall Speed (X_6)

The terminal fall speed of graupel is calculated according to the *Böhm* [1989] formulation:

$$V_g = \frac{\mathrm{Re}\eta}{2\rho_a}\left(\frac{\pi}{A}\right)^{1/2},$$

where Re is the Reynolds number, η is the kinematic viscosity, ρ_a is the air density, and A is the circumscribed area defined as the area of the smallest circle or ellipse that completely contains the effective projected area. The Reynolds number is related to the Best number through $X = C_D\mathrm{Re}$, where C_D is the drag coefficient. There are therefore several sources of uncertainty in the terminal fall speed: the graupel density, the effective projected cross-sectional area, the circumscribed area, and the relationship between the Reynolds number and the Best number. *Heymsfield and Wright* [2014] showed that the roughness can cause large differences in values of the Reynolds number for any given Best number across the whole domain, regardless of the graupel size. The Reynolds number for graupel due to its relationship with the Best number is multiplied by a factor between 0.5 and 2 in our study. For simplicity, this parameter is referred to as the graupel aerodynamic parameter in the following text. Although both the graupel density (X_1) and the aerodynamic parameter (X_6) affect the terminal fall speed, the values of these two parameters are not correlated.

2.2.7. Collection Efficiency of Drops by Graupel (X_7) and of Ice Crystals by Graupel (X_8)

Factors such as the size and shape of graupel, the relative collision velocity and drop sizes can all affect the collection efficiency [*von Blohn et al*., 2009]. Furthermore, the graupel-drop collision kernels may significantly increase in turbulent clouds [*Khain et al*., 2000; *Wang et al*., 2005], and the degree by which the collection efficiency depends on temperature, humidity, and other atmospheric parameters is also unknown. The efficiency is dimensionless. In our study, the collection efficiency of drops by graupel is multiplied by a factor between 0.01 and 10, while the collection efficiency of ice crystals by graupel is multiplied by a factor between 0.1 and 3.

2.2.8. Capacitance of Ice Crystals (X_9)

Ice crystals have various habits and are generally not spherical in shape. The supersaturation just above the growing surface of a nonspherical crystal is not as uniform as in the far field. The deposition/evaporation equation for crystal growth has to be modified to include the effect of crystal habit. A common method to consider the nonspherical effect is to introduce the analogy between the diffusion of heat and water vapor around a crystal to that of electrical charge dissipation from a capacitor of similar shape [*Cotton et al*., 2011]. In this way, theoretical capacitances for some simple shapes of crystals can be derived [*McDonald*, 1963]. There is uncertainty in capacitance. For example, *Westbrook et al*. [2008] found that the capacitance of an aggregate is close to half of the value for a sphere, while *Bailey and Hallett* [2012] argued that theoretical estimates of capacitance overestimate the actual growth by a factor of 2–4. *Lamb and Verlinde* [2011] recognized that it is realistic only if both the particle mass and the aspect ratio can be calculated simultaneously. The uncertainty in the capacitance parameter is set to be a factor between (0.01, 10).

2.2.9. The Concentration of the Aitken and Accumulation Modes of Aerosol (X_{10})

Aerosol particle concentrations exert a strong influence on the development of cloud microphysics, precipitation, and dynamics [*Rosenfeld et al*., 2008; *Koren et al*., 2008; *Kaufman et al*., 2005]. Rather than being an uncertain parameter, aerosols constitute a variable forcing on clouds. We include the specification of aerosol particle concentrations as an uncertain model input here in order to understand the effect on cloud microphysics relative to the uncertain model parameters. In MAC3, the initial aerosol size distribution is expressed as a combination of three modes (Aitken, accumulation, and coarse) of lognormal distributions. The total numbers of aerosol particles in the Aitken and accumulation modes are changed by a factor between 0.01 and 4 in our study, leading to a range of concentration of the two aerosol modes from

Table 2. The Output Variables Considered, with Summary Statistics for Each Output Obtained From the Simulated Uncertainty Distributions Over the Full Parameter Space in Figure 5[a]

Model Output (Units)	Min	LQ	Median	UQ	Max	μ	σ	$\lvert\frac{\sigma}{\mu}\rvert$
Mean effective radius (μm)	3.62	180.37	225.09	264.60	457.15	224.10	66.34	0.30
Mean updraught speed (m s^{-1})	1.98	3.26	3.56	3.78	5.00	3.49	0.46	0.13
Mean downdraught speed (m s^{-1})	−7.33	−6.01	−5.48	−4.58	−1.54	−5.22	1.08	0.21
Mean value of specific drop mass (g kg^{-1})	0.31	0.77	0.92	1.04	1.54	0.90	0.19	0.21
Mean value of specific ice crystal mass (g kg^{-1})	0.04	0.35	0.51	0.73	1.65	0.56	0.27	0.48
Mean value of specific graupel mass (g kg^{-1})	0.01	1.02	1.35	1.64	2.73	1.27	0.54	0.42
Mean drop number concentration (cm^{-3})	2.15	9.77	26.70	76.19	329.51	53.13	59.99	1.13
Mean ice crystal number concentration (L^{-1})	0.49	39.31	94.09	205.52	3810.87	177.54	262.25	1.48
Mean graupel number concentration (L^{-1})	0.01	0.24	0.97	1.98	31.16	1.73	2.64	1.52
Mean reflectivity (dBZ)	14.43	47.14	51.66	58.67	67.54	51.53	8.75	0.17
Accumulated precipitation at 80 min (mm)	0.00	12.09	18.88	35.38	72.54	23.48	16.42	0.70
Maximum precipitation rate (mm h^{-1})	0.00	65.56	99.78	192.38	852.97	152.69	145.28	0.95

[a]The summary statistics included are the minimum (Min), lower quartile (LQ), median, upper quartile (UQ), maximum (Max), mean (μ), and standard deviation (σ) from the distributions, along with an estimate of the relative uncertainty for each case given by $|\sigma/\mu|$.

approximately 50 to 20,000 cm^{-3}, which covers more than the typical range of aerosol concentrations and is somewhat larger than used in *Cui et al*. [2006].

2.2.10. The Concentration of the Coarse Mode of Aerosol (X_{11})

The measurement of coarse mode aerosol is even more variable than that of the Aitken and accumulation modes [e.g., *Reid et al*., 2006]. This parameter defines the total number of coarse mode aerosol particles in the initial size distribution. The total number of aerosol particles in the coarse mode is changed by a factor between (0.01, 100) in our simulations, resulting in particle concentrations in the range 0.0045–4.5 cm^{-3}.

Together, these defined uncertainty specifications form an 11 dimensional parameter uncertainty space over which we want to evaluate outputs from the cloud microphysics model. We aim to assess how this uncertainty propagates through the model to each of a selection of model outputs in order to determine which input parameters, and hence corresponding processes and mechanisms, drive uncertainty in the cloud responses of interest.

2.3. Choice of Model Outputs

For each model run, we have simulated 80 min of cloud formation and development and recorded 12 model outputs, defined in Table 2. The selection of outputs encompasses cloud dynamical responses, cloud particle responses, and precipitation. The outputs are summary statistics taken over space and time through the centre of the cloud. It would also be possible to analyze outputs at a particular time in the cloud development, or at a specific location in the cloud. However, each cloud evolves differently depending on the parameter setting, so it is difficult to compare sensitivities without averaging in time and space.

3. Statistical Methods

In this study, we use variance-based sensitivity analysis to determine which input parameters, and therefore model processes and mechanisms, lead to parametric uncertainty in the MAC3 model outputs of interest. Evaluation of the corresponding model sensitivity measures, and so the effects of input parameter uncertainty on model outputs, is classically achieved using a direct Monte Carlo simulation approach. This involves running the model simulator many times over different combinations of input parameter values, but when the model is computationally expensive to run like MAC3 these calculations can quickly become unfeasible. Instead, we take advantage of the Bayesian statistical theory for building fast surrogate computer models, known as emulation, to construct surrogate representations of MAC3 that can be used in place of the model simulator itself to make these calculations. This structured Bayesian approach to evaluating model sensitivity, originally proposed by *Oakley and O'Hagan* [2004] and as depicted by the flow diagram in *Lee et al*. [2011, Figure 1], requires us first to generate a designed set of well-spaced training runs from MAC3 over the defined parameter uncertainty space. Then, through the application of Gaussian process emulation over this training data to each MAC3 model output independently, we are able to evaluate

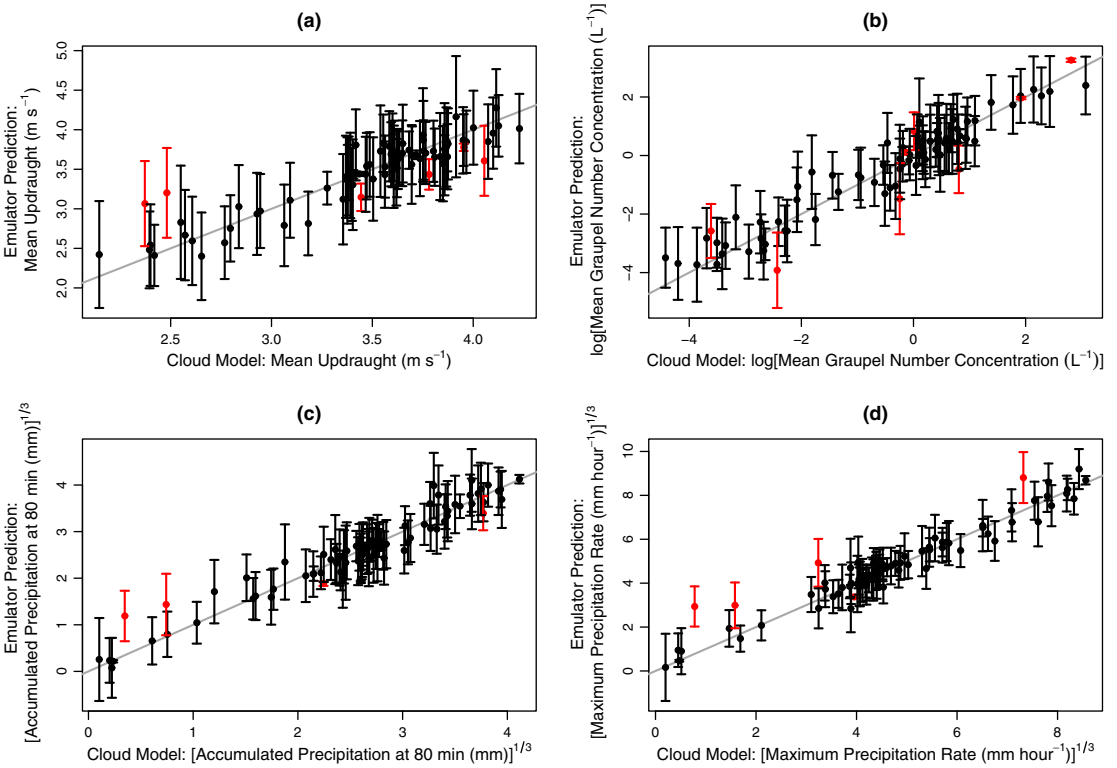

Figure 1. Emulator validation for the cloud responses (a) mean updraught, (b) mean graupel number concentration, (c) accumulated precipitation at 80 min, and (d) maximum precipitation rate. In each case, the MAC3 model output (*x* axis) is plotted against the corresponding emulator prediction (*y* axis) for the model runs of the validation data set, with 95% confidence bounds on the emulator predictions. The gray line is a line of equality and runs where the model output has not been captured within the 95% confidence bounds of the emulator prediction are shown in red. Plots (b)–(d) are displayed on the transformed output scales on which the emulator models are fitted.

these model outputs across all dimensions of the parameter uncertainty space at a very low computational cost, making the variance-based sensitivity analysis of MAC3 possible.

In this section, we outline the statistical methods that come together to form this structured Bayesian approach, and we describe how each one has been applied in our analysis of MAC3.

3.1. Statistical Design for the Training Data

The aim of our sensitivity study is to determine how the defined uncertainty in each of the eleven input parameters from section 2.2 feeds through MAC3 to affect each model output of interest. Therefore, each emulator model we construct must cover the full parameter space defined by these uncertain input parameters.

Emulator training data are obtained by running a set of chosen input combinations $\mathbf{x}=\{\boldsymbol{x_1}, \boldsymbol{x_2}, \ldots, \boldsymbol{x_n}\}$, where $\boldsymbol{x_i}=\{x_{i,1}, \ldots, x_{i,11}\}$, through the cloud model simulator to obtain the corresponding model outputs $\boldsymbol{y}=\{y_1, y_2, \ldots, y_n\}$. The number of training runs n required to achieve a reasonable model fit for the emulator is dependent on the number of active input parameters and how smoothly the simulator output varies over the parameter space. A common practice, as discussed and supported by *Loeppky et al.* [2009], is to use $n=10d$ runs from the model simulator for training the emulator (where d is the number of uncertain input parameters over which the emulator is to be built), with the premise that more model runs can be added to the training data if it is found through diagnostic checks that the emulator accuracy is poor. Consequently, we use $n = 110$ training runs for the MAC3 emulation here.

To achieve an optimal coverage of the parameter space with these 110 emulator training runs, we use a space filling statistical experiment design method to choose the actual input combinations $\mathbf{x}$. One of the most widely used design algorithms for this purpose is the maximin Latin hypercube [*Morris and Mitchell*, 1995], and this is the method we have used for our training data here. The maximin Latin hypercube

algorithm maximizes the minimum distance between points in order to ensure optimum space filling and hence a good coverage of the parameter uncertainty space.

3.2. Emulation

Emulation is a technique by which we construct a statistical representation—an *emulator*—of a particular aspect of a model simulator (such as the relationship between a set of uncertain inputs and an output of interest) that can be evaluated quickly. The approach stems from the work of *O'Hagan* [1978] who described how a Gaussian process can be used to represent an unknown function. The methodology has since been further developed and applied within the literature [see e.g., *Sacks et al.*, 1989; *Kennedy and O'Hagan*, 2001; *Oakley and O'Hagan*, 2004; *Lee et al.*, 2013]. In this study, we adopt the most common emulator form, using the Gaussian process as the basis of our emulator models. A mathematical description of Gaussian process emulation is given in Appendix A, and here we describe the application of the Gaussian process emulator to MAC3.

The model outputs from MAC3 are considered independently in this work, so a separate emulator is constructed for each model output Y. In each case, we represent the cloud model simulator as a function $\eta(\cdot)$ of the 11 uncertain input parameters $\mathbf{X}=\{X_1,\ldots,X_{11}\}$ over the parameter uncertainty space such that $Y=\eta(\mathbf{X})$. An emulator is then constructed to represent the input-output relationship using Bayesian statistical theory by combining the information from the model simulator in the training data with a set of prior beliefs about the behavior of MAC3. These prior beliefs are characterized in the form of a Gaussian process with a specified mean and covariance structure, $m(\cdot)$ and $V(\cdot,\cdot)$, respectively, as detailed in Appendix A. For the 12 emulators here, a linear mean structure for the output with respect to all uncertain input parameters given by:

$$Y=m(\boldsymbol{x})=C+\sum_{i=1}^{11}\beta_i x_i$$

is assumed, where C is a constant term and the β_i are unknown linear regression coefficients that are estimated in the model fit, along with a Matérn covariance structure for $V(\boldsymbol{x},\boldsymbol{x}')$. The Matérn covariance structure was chosen as this form has been found to cope more easily with any slight roughnesses in the model output surface [*Rasmussen and Williams*, 2006], and it could easily be the case that the model output surface is not completely smooth for some of the cloud properties from MAC3.

This posterior model is the emulator, defining a fitted surface with uncertainty for the model output Y over the 11 dimensional parameter uncertainty space. We note that even though the prior mean takes a linear form here, the posterior Gaussian process is not restricted by this and can take a quite different nonlinear form, dependent on the information from the training data. The fitted surface passes through each of the training data points exactly, and given the derived mean and covariance structure, the emulator interpolates the output Y over the parameter space to provide an estimate of Y at all untried points along with a measure of uncertainty about this prediction.

Each emulator was fitted using the statistical software R [*R Core Team*, 2013], and the R package DiceKriging [*Roustant et al.*, 2012]. In order to avoid erroneous predictions from the emulator when a model output has a natural lower bound at zero it was necessary to transform some of the cloud model outputs prior to fitting the emulator. In the results that follow, the outputs for the mean number concentrations of drops, ice crystals, and graupel are emulated using the natural logarithm transform given by $Z_i=\log_e(Y_i)$, and the outputs for the mean ice crystal mass, the mean graupel mass, the accumulated precipitation at 80 min and the maximum precipitation rate are emulated using the cube root transform given by $Z_i=\sqrt[3]{Y_i}$. Nonetheless, in all of these cases the uncertainty and sensitivity analysis of the output variable is evaluated on the original output scale via back-transform of the emulator predictions prior to calculation of the uncertainty and sensitivity measures. Such transforms do have the effect of inflating the standard errors (uncertainty) about the emulator predictions on back-transformation. However, it is the mean prediction from the emulator that we take forward and use for our sensitivity analysis and we have found that this is robust to this error inflation.

3.3. Emulator Validation

The process of validation to assess the fit of an emulator model is important as there is no guarantee that the training data set $(\mathbf{x};\boldsymbol{y})$ used to construct the emulator is sufficient to describe the output at other locations within the parameter uncertainty space. The validity of the fitted emulator model for each of the 12 cloud model outputs has been assessed using a selection of the methods and diagnostics detailed in *Bastos*

and O'Hagan [2009]. For validation, a second set of MAC3 model runs was evaluated, which we refer to as the *validation data*. This validation data contains model runs for 88 input combinations that are different to those contained in the training data. Ten of the input combinations were selected to be specifically close to training data points in the parameter space and the remainder were selected using the maximin Latin hypercube experiment design algorithm to ensure good coverage of the whole parameter uncertainty space in the validation. We select specific points within close proximity to the emulator training runs as well as points further away within the parameter uncertainty space as the evaluation of each of these can inform us about different aspects of the fit of the emulator. For example, points close to design runs can be highly sensitive to the hyper-parameters of the estimated correlation function within the covariance structure of the emulator model [*Bastos and O'Hagan*, 2009].

Figure 1 shows validation plots for a selection of the cloud responses: the mean updraught, the mean graupel particle number concentration, the accumulated precipitation at 80 min, and the maximum precipitation rate. These plots are scatterplots of the emulator mean predictions versus the actual MAC3 model output for the validation data set, with 95% confidence intervals on the emulator mean predictions calculated via the posterior emulator covariance structure given by equation (A3) in Appendix A. Figure 1 shows the true MAC3 model output to lie within the 95% confidence bounds of the emulator prediction for the vast majority of the validation runs. Where this is not the case, the points are highlighted in red. Looking across all 12 cloud responses, the total percentage of the validation runs for which the MAC3 model output lies outside the 95% confidence bounds of the corresponding emulator prediction for any one output is no higher than 10%, and for many of the outputs this is much lower at around 5%, which we expect to be the case given we are using a 95% confidence bound for this diagnostic. For each model output in Figure 1, the plotted points follow reasonably close to the line of equality depicted in gray. We also see this in the corresponding validation plots for the further eight model outputs that are not shown here. This indicates that across all outputs the emulator mean prediction is providing a reasonable representation of the actual model output from MAC3.

The overall uncertainty in a model output Y can be broken down into two components: the parametric uncertainty (caused by the uncertainty in the model parameters, $\mathbf{X}$) and the emulator uncertainty (the consequence of using the emulator rather than the model itself to evaluate Y). For the emulator to be useful and capture the model signal with reasonable precision, we require the emulator uncertainty to be less than the parametric uncertainty that we are aiming to quantify. Both the emulator uncertainty and the parametric uncertainty can be estimated through the simulation of Gaussian process functions from the emulator model. On comparison, we have found that the magnitude of the emulator uncertainty ranges between 2.5% and 5.2% of the magnitude of the parametric uncertainty for the MAC3 model outputs considered in this study. This shows that in comparison to the overall parametric uncertainty in the model outputs, the uncertainty due to the emulator approximation itself is minimal.

Additional validation diagnostics to assess the model fit for each emulator have been implemented and examined, including the leave-one-out approach detailed in *Rougier et al*. [2009], the evaluation of standardized model residuals and the analysis of the pivoted Cholesky variance decomposition as proposed by *Bastos and O'Hagan* [2009]. The resulting diagnostic plots from these further validations (not shown) support our conclusions here that each emulator is providing a reasonable representation of its corresponding cloud response over the parameter uncertainty space. We therefore consider each of the fitted emulator models as valid in this study, and take them forward to use in place of MAC3 for the calculation of our uncertainty and sensitivity measures.

3.4. Sensitivity Analysis

Sensitivity analysis methods provide a mechanism through which the variation in a model output can be decomposed and proportionally assigned to different contribution sources. Given an understanding of the uncertainty in a set of model input parameters, it is possible via sensitivity analysis to quantify the effect of this uncertainty on a model output of interest and determine which input uncertainties drive the variation in that output. A comprehensive overview of methods for sensitivity analysis is given by *Saltelli et al*. [2000].

To assess the sensitivity of the MAC3 model to the set of 11 uncertain input parameters defined in section 2.2, we apply the approach of probabilistic variance-based sensitivity analysis. This approach allows us to measure the sensitivity of a model output, be it a linear or a nonlinear model response, to both individual input parameters and interaction effects simultaneously across the full parameter uncertainty space. The

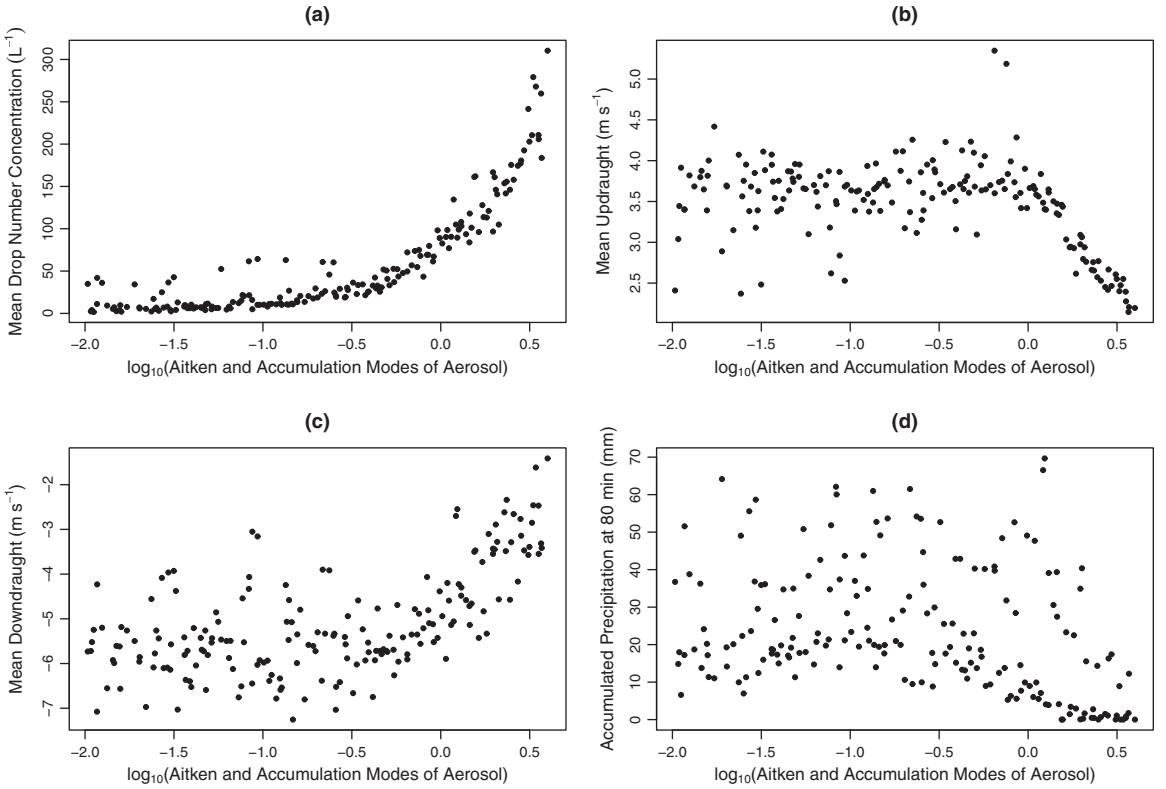

Figure 2. Pairwise scatterplots of the emulator training and validation model runs for (a) mean drop number concentration, (b) mean updraught, (c) mean downdraught, and (d) accumulated precipitation at 80 min (*y* axis), versus the scaled Aitken and accumulation modes of aerosol concentration (*x* axis). $\text{Log}_{10}(X_{10})=0$ corresponds to an Aitken and accumulation mode aerosol concentration of approximately 5000 cm^{-3}.

methodology is based on the decomposition of the overall variance of an output into contributions from individual inputs and combinations of inputs together. The resulting variance decomposition is used to compute two sensitivity measures: the *main effect index* and the *total effect index*, as detailed in *Saltelli et al*. [2000], and summarized in Appendix B. For each uncertain input parameter of MAC3, the main effect index provides a measure of the percentage by which the overall variance in the cloud model output *Y* could be reduced if the input parameter was known exactly. The total effect index provides a joint measure of the individual effect of an input parameter and all interaction effects that involve that specific input. Hence, the difference between the total effect index and the main effect index gives an indication of how much an input parameter is interacting with other inputs in the cloud model. Given the complex microphysics involved in the formation of a cloud, it is possible that there may be some strong interaction effects between the uncertain input parameters for the MAC3 model outputs under investigation here.

Evaluation of the variance-based sensitivity measures for each model output from MAC3 requires many evaluations of the output over the parameter uncertainty space. Here we use the constructed emulators in place of MAC3 and sample across the parameter uncertainty space using the extended-FAST (Fourier Amplitude Sensitivity Test) approach of *Saltelli et al*. [1999] in order to compute the sensitivity measures. The extended-FAST approach to the sampling is specifically designed for sensitivity analysis, and it generates a much more efficient sample across the parameter space in comparison to the general Monte Carlo sampling approach. The calculations of the sensitivity measures for this study have been completed using the R package "sensitivity" [*Pujol et al*., 2013], and the results of this sensitivity analysis are discussed in section 4.3.

4. Results

4.1. Exploratory Analysis of the Training and Validation Model Runs

To begin our analysis of how the uncertainty in the MAC3 model input parameters affects the model outputs of interest, we explore pairwise scatterplots of the emulator training and validation model runs for all

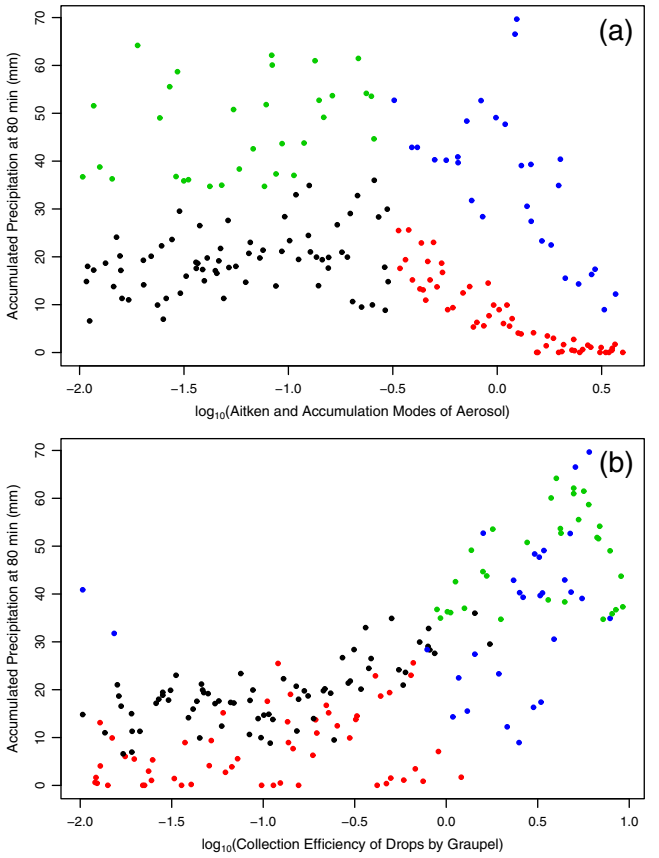

Figure 3. Pairwise scatterplots of the model runs for the accumulated precipitation at 80 min (*y* axis) versus (a) the Aitken and accumulation modes of aerosol, and (b) the collection efficiency of drops by graupel (*x* axis), showing a breakdown by different cloud behaviors in color: Regime R1 in black, Regime R2 in red, Regime R3 in green, and Regime R4 in blue.

input/output combinations. Examination of these plots has revealed that the parameter corresponding to the concentration of the Aitken and accumulation modes of aerosol has the most influence across the cloud properties we consider. Figure 2a shows the strongest pairwise relationship that was found, between the concentration of the Aitken and accumulation mode aerosol and the mean drop number concentration. (We note here that the range of values taken by this aerosol parameter is on a multiplicative scaling, so a $\log_{10}$ transform is used for the plotting. The model default value from which the parameter is varied within this study corresponds to a value of $\log_{10}(X_{10})=0$.) We see in Figure 2a that as the $\log_{10}$ scaling of the aerosol concentration increases, the mean drop number concentration increases exponentially. Hence, the drop number concentration increases approximately linearly with the aerosol scaling itself.

Figures 2b and 2c show the effect of the concentration of the Aitken and accumulation mode aerosol on the mean updraught and mean downdraught in the simulated cloud, respectively. These plots show that the cloud behavior changes distinctly for the higher aerosol concentrations, with these vertical velocities (and hence the formed cloud) decaying away as the aerosol concentration becomes large. This change in cloud behavior occurs at approximately $\log_{10}(X_{10})=-0.5$, which corresponds to a Aitken and accumulation mode aerosol concentration of 0.32× the default value, or approximately 1600 cm^{-3}. Figure 2d shows that this change feeds through to the precipitation response from the cloud. Via close examination of Figure 2d, we have identified four groupings of the cloud precipitation output, which are highlighted in color in Figure 3a. The points colored black (lower aerosol) and red (higher aerosol), show a pattern in the precipitation response to the aerosol that is well known [*Cui et al.*, 2011a]. At low aerosol concentrations the accumulated precipitation is reasonably stable, but as the aerosol concentration is increased to represent a strongly polluted environment (red points), the precipitation decreases sharply (Figures 2b and 2c). This same overall pattern also occurs for much higher precipitation totals as shown by the green and blue points in Figure 3a. These points correspond to high settings of the collection efficiency of drops by graupel particles, which is shown in Figure 3b. In the rest of the paper, we refer to these regimes as follows:

Regime R1 (black points) corresponds to low aerosol concentration ($\log_{10}(X_{10}) < -0.5$; Aitken and accumulation mode concentration <1600 cm^{-3}) and low collection efficiency of drops by graupel ($\log_{10}(X_7) < 0$);

Regime R2 (red points) corresponds to high aerosol concentration ($\log_{10}(X_{10}) > -0.5$) and low collection efficiency of drops by graupel ($\log_{10}(X_7) < 0$);

Regime R3 (green points) corresponds to low aerosol concentration ($\log_{10}(X_{10}) < -0.5$) and high collection efficiency of drops by graupel ($\log_{10}(X_7) > 0$); and

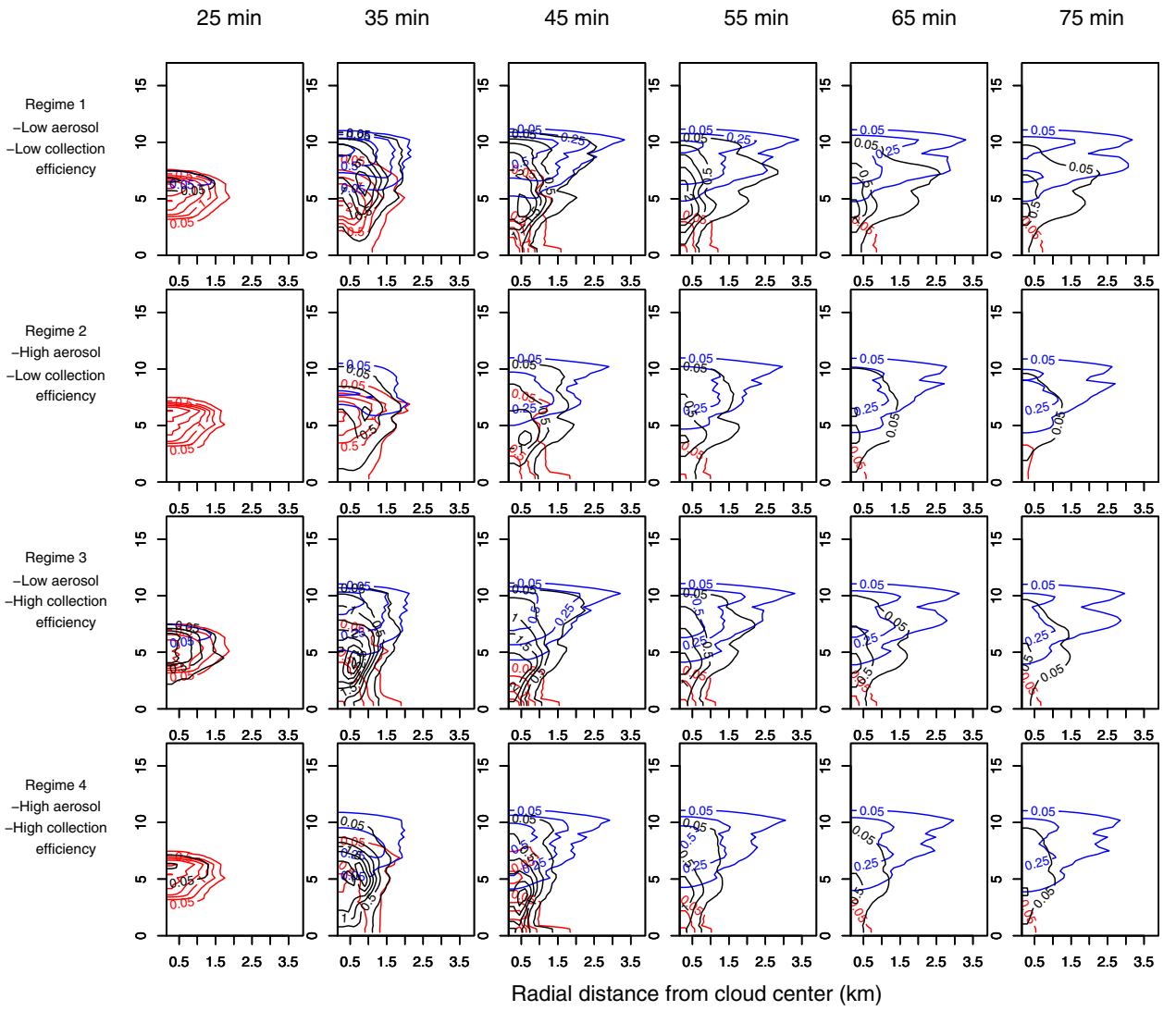

Figure 4. Time sequence of the averaged specific mass contents (g m^{-3}) of the simulated clouds from 25 to 75 min at 10 min intervals for each of the four regimes as defined in Figure 3 and section 4.1. The *x* and *y* axes are radial distance from cloud center (km) and altitude (km), respectively. Red lines correspond to drops, blue lines correspond to ice crystals, and black lines correspond to graupel particles. Across the particle types, contours for mass contents of 0.05, 0.25, 0.5, 1, 1.5, 2, and 2.5 g m^{-3} are shown.

Regime R4 (blue points) corresponds to high aerosol concentration ($\log_{10}(X_{10}) > -0.5$) and high collection efficiency of drops by graupel ($\log_{10}(X_7) > 0$).

Figure 4 depicts the average simulated cloud as it develops over time from each of these defined cloud behaviors. There are visible differences in the four regimes. Generally, the graupel masses are higher in regimes of high collection efficiency (R3 versus R1 and R4 versus R2) and higher in regimes of low aerosol (R1 versus R2 and R3 versus R4). Correspondingly, precipitation is heavier in regimes of high collection efficiency and regimes of low aerosol. Furthermore, precipitation starts earlier in the regimes of high collection efficiency (R3 versus R1 and R4 versus R2). It is possible that the drivers of uncertainty for the model outputs of interest may be different within each of these defined regimes and also different in comparison to when we evaluate the drivers of uncertainty with respect to the whole parameter uncertainty space. This will be considered further in section 4.3.

4.2. Uncertainty in the Cloud Responses

Figure 5 shows a histogram of the uncertainty in each cloud output due to the defined parametric uncertainty in the MAC3 model inputs from section 2.2, generated by Monte Carlo simulation over the whole

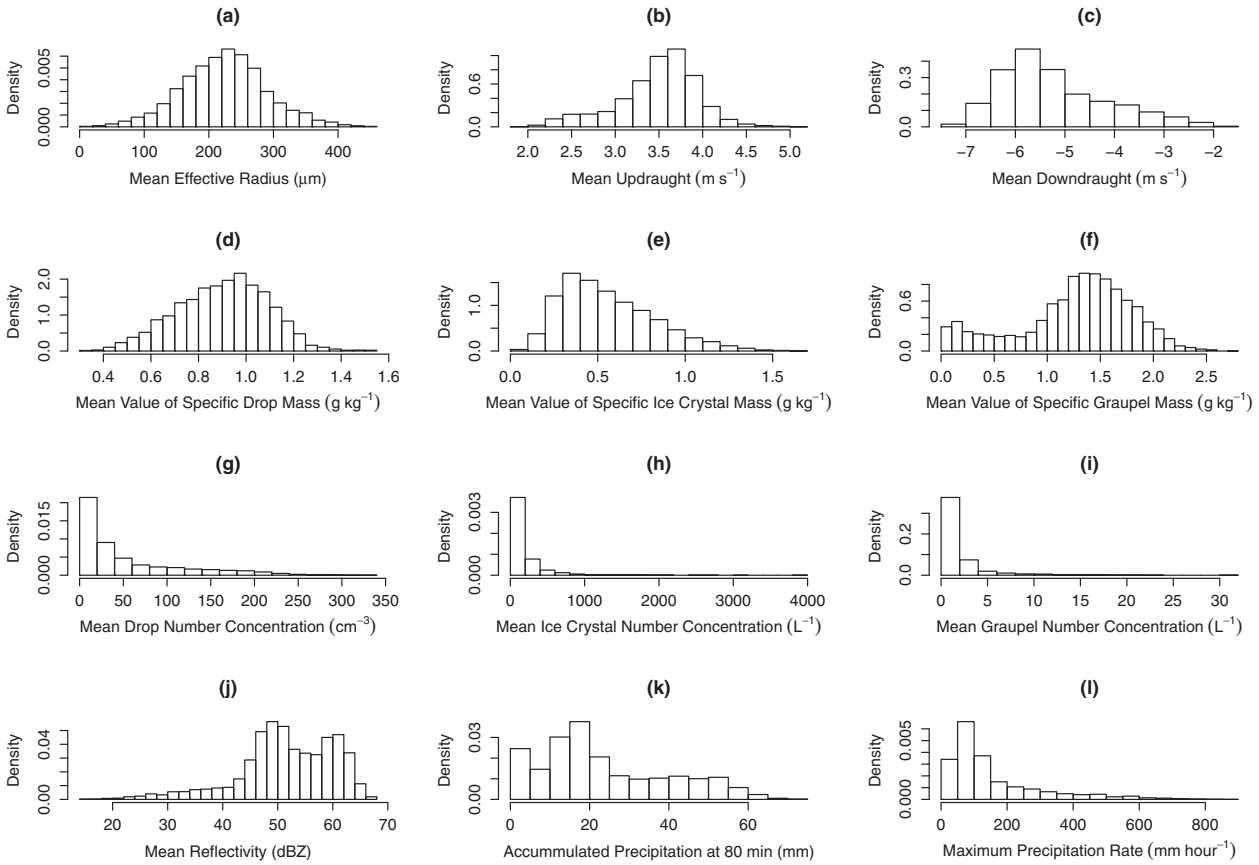

Figure 5. Histograms of the uncertainty in each cloud response due to the propagation of the parametric uncertainty in the input parameters through the MAC3 model.

parameter uncertainty space using the emulator. Here we assume a uniform distribution across the defined range of values for each uncertain input parameter and use a sample size of 5500 input combinations in each case. The shape of the uncertainty distribution changes depending on the cloud response considered, and many of the simulated distributions show a degree of skewness. Figures 5g–5i show that the mean particle number concentrations of drops, ice crystals, and graupel particles in the cloud vary exponentially, and the range of possible values for the mean number concentration of ice crystals is extremely large. The uncertainty in the precipitation responses (Figures 5k and 5l) is positively skewed, and we also note that there is a second mode in the distribution for the accumulated precipitation at low values. This may be caused by the identified regime changes in the simulated cloud from section 4.1, with the low peak in the distribution likely corresponding to clouds from Regime R2 (Figure 3, red points) with high aerosol and low collection efficiency of drops by graupel particles.

Table 2 contains summary statistics for each output, calculated from the simulated uncertainty distributions in Figure 5. These include the minimum, lower quartile, median, upper quartile, and maximum values from the distribution, the mean value (μ), and the standard deviation (σ). These statistics provide an overview of the absolute uncertainty generated in each cloud response as a result of the defined uncertainty in the model input parameters, showing the absolute spread of values as well as a further indication of the amount of skewness in the output distribution given by the difference in the mean and median values. The final column gives the relative uncertainty, calculated as $|\sigma/\mu|$, which indicates which outputs show the most variation relative to the mean value in their respective uncertainty distributions.

From both Figure 5 and Table 2, the mean drop number concentration, the mean ice crystal number concentration, and the mean graupel number concentration are the most uncertain of the cloud responses, with values of $|\sigma/\mu| > 1$ corresponding to a standard deviation that is greater than 100% the magnitude of the mean value. In absolute terms the mean ice number concentration is the most variable of these cloud

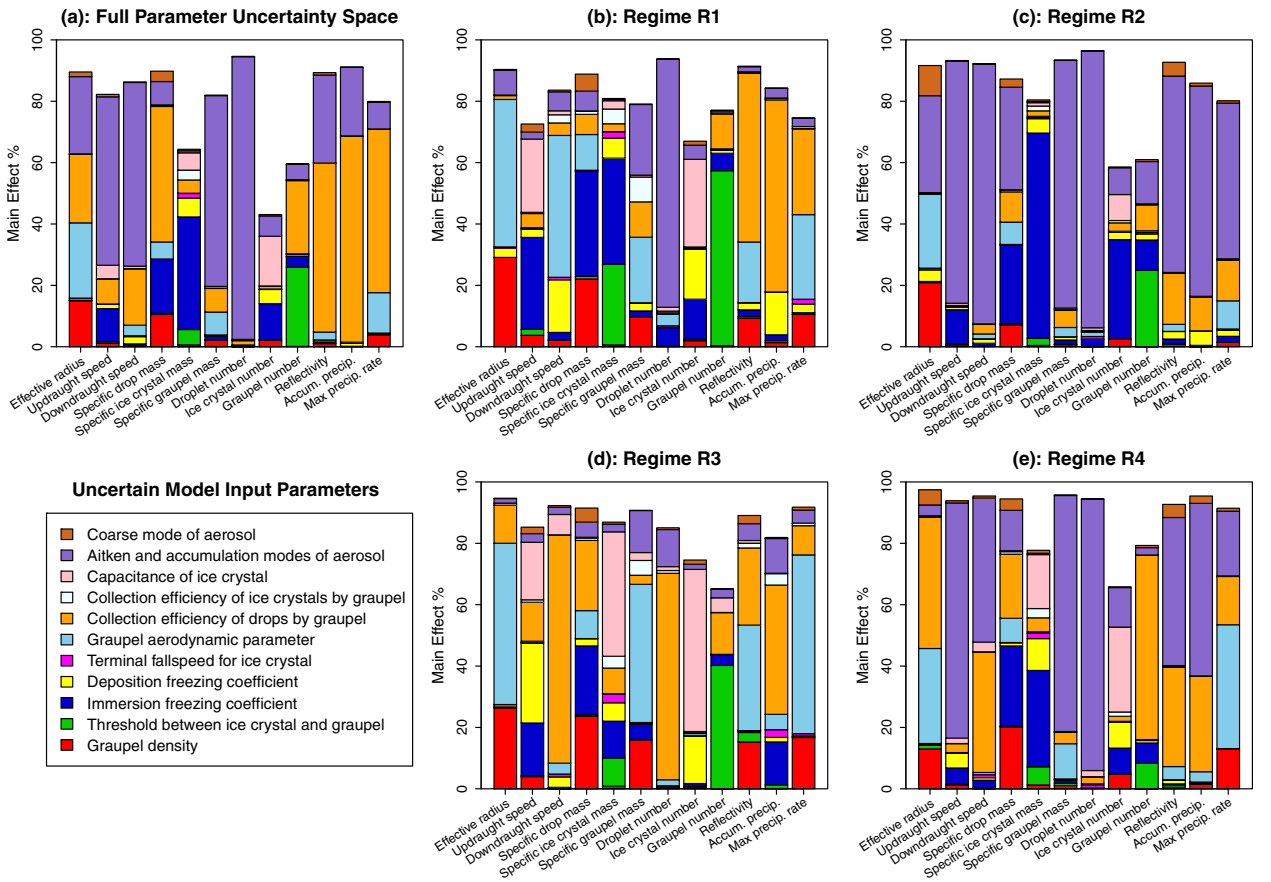

Figure 6. The main effect sensitivity results evaluated for all cloud responses (a) given the full parameter uncertainty space, (b) for Regime R1 (low concentration of Aitken and accumulation modes of aerosol, X_{10}, and low collection efficiency of drops by graupel, X_7), (c) for Regime R2 (high X_{10} and low X_7), (d) for Regime R3 (low X_{10} and high X_7), and (e) for Regime R4 (high X_{10} and high X_7).

responses, with the range of possible values covering both extremes of a very low concentration of ice crystals in the cloud at a minimum value of approximately 0.5 L^{-1}, to a cloud that is completely dominated by ice crystals at a maximum value of approximately 3800 L^{-1}. However, in relative terms it is the mean graupel number concentration that shows the largest spread relative to the mean value, with a standard deviation that is more than 150% the magnitude of the mean value. The cloud response that varies the least relative to the mean value is the mean updraught. The relative uncertainty estimates for the precipitation responses indicate that there is more uncertainty across the parameter uncertainty space in the maximum precipitation rate than in the amount of accumulated precipitation at 80 min.

4.3. Sensitivity Study

To determine which factors and processes are controlling the uncertainty in the model outputs, we performed a variance-based sensitivity analysis with respect to each of the cloud model outputs individually. In each case, we have calculated the main effect and total effect sensitivity measures using the formulae from equations (B2) and (B4) in Appendix B, respectively.

Figure 6 shows stacked bar charts of the main effect sensitivity results for the 12 model outputs when the sensitivity of the outputs is evaluated across the whole parameter space and separately in each of the regimes defined by the setting of the aerosol and collection efficiency parameters. We can infer from the plots in Figure 6 that the model output uncertainty is mainly driven by the first order main effects for the majority of the cloud responses, with at least 80% of the uncertainty attributed to main effects for around nine of the 12 outputs in each case. Where the height of the stacked bar is less than 100%, this indicates that there are interaction effects providing more significant contributions to the output uncertainty. In particular, we see that this occurs for the mean value of specific ice crystal mass and the mean number

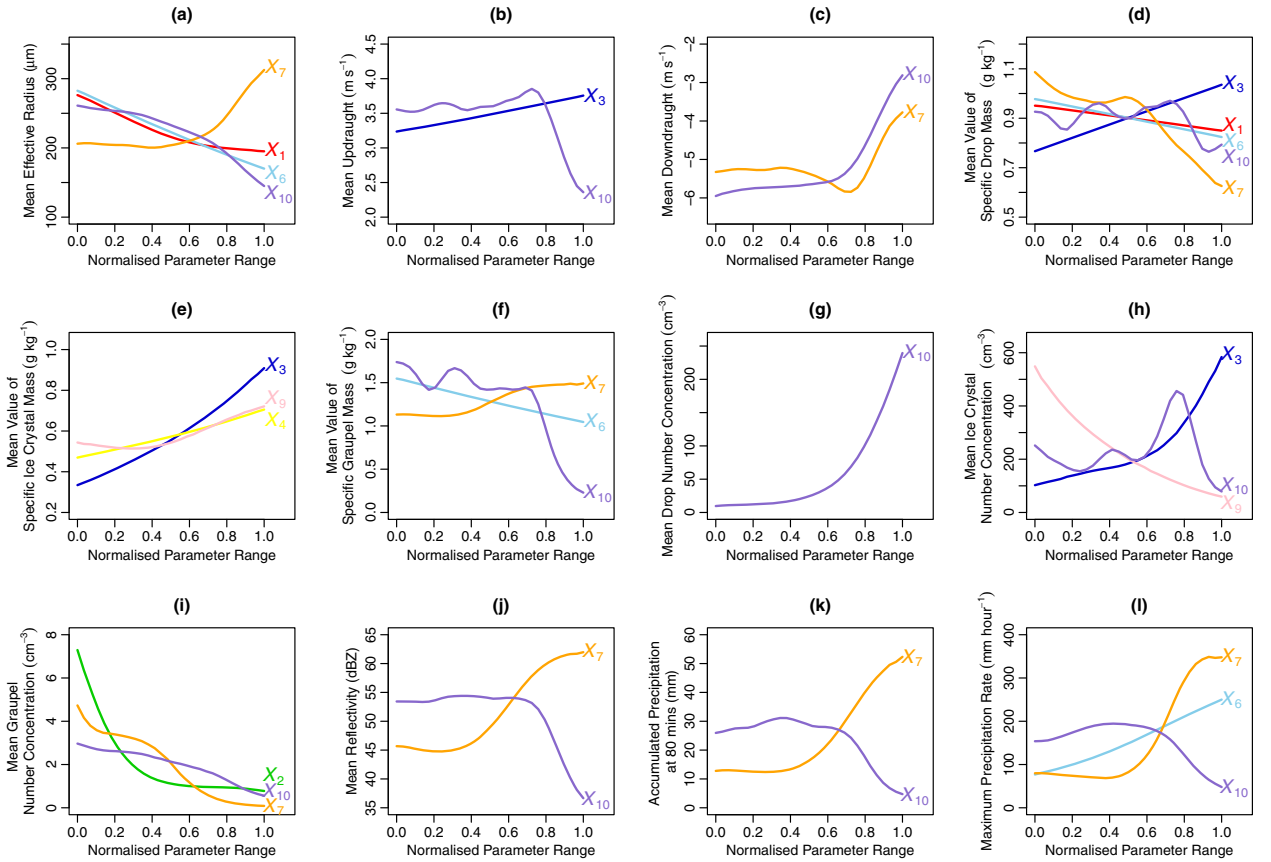

Figure 7. The most significant main effects for each model output from the sensitivity analysis over the full parameter uncertainty space (Figure 6a), for which the corresponding contribution to the uncertainty in the model output is greater than 5%. The main effects are colored according to the legend of Figure 6, where X_1 is the graupel density, X_2 is the threshold between ice crystal and graupel, X_3 is the immersion freezing coefficient, X_4 is the deposition freezing coefficient, X_6 is the graupel aerodynamic parameter, X_7 is the collection efficiency of drops by graupel, X_9 is the capacitance of ice crystal, and X_{10} is the Aitken and accumulation modes of aerosol.

concentration of both ice crystals and graupel particles. Figure 7 displays the largest, and therefore most significant, main effects from the sensitivity analysis over the full parameter uncertainty space, showing how the model outputs are responding to the perturbation of these parameters over their uncertainty ranges. Main effects are included in Figure 7 if the corresponding contribution to the uncertainty in the model output is greater than 5%. The model output response is essentially flat for parameters not included, where the uncertainty contribution is less than 5%. Below we examine the main factors controlling uncertainty in the different cloud responses and we discuss the implications of these findings.

4.3.1. The Precipitation Responses

Figure 6 shows that the important contributors to the uncertainty in the maximum precipitation rate are the collection efficiency of drops by graupel, the graupel aerodynamic parameter, the concentration of the Aitken and accumulation mode aerosol, and the graupel density. Since the mass of a drop is proportional to the cube of its radius, the amount of precipitation is controlled mostly by large drops. It has been shown that the precipitation in midlatitude convective clouds is mainly due to the melting of the rimed graupel particles [*Cui et al.*, 2011a]. The rimed mass of a graupel particle depends on the concentration of drops to be captured, the sweeping volume and the collection efficiency. The concentration of drops is generally controlled by the Aitken and accumulation modes of aerosol, whereas the sweeping volume is a function of the terminal fall speed of the graupel and the sweeping area, which are influenced by the graupel density and the graupel aerodynamic parameter.

The relative sizes of the uncertainty contributions from the different parameters varies both between the analysis over the full parameter uncertainty space (Figure 6a) and the analyses over the four separate regimes (Figures 6b–6e), and from regime to regime. When we consider the uncertainty across the full

parameter space (Figure 6a), the variation in the parameter for the collection efficiency of the drops by graupel particles very much drives the uncertainty in the maximum precipitation rate. However, within each regime this parameter is much less influential. In regime R1 (Figure 6b), where the resource of aerosol to be collected is low, the main contributions to the uncertainty in the maximum precipitation rate come from the uncertainty in the sweeping volume (which is driven by the graupel aerodynamic parameter and the graupel density) as well as the collection efficiency. In regime R2 (Figure 6c), the parameter relating to the concentration of the Aitken and accumulation modes of aerosol has the largest influence on the output uncertainty, with the parameters corresponding to the collection efficiency and the sweeping volume being secondary. For regimes R3 and R4 with high collection efficiency (Figures 6d and 6e), the sweeping volume parameters provide the largest contribution to the uncertainty, with smaller contributions from the aerosol and collection efficiency.

The main drivers of the uncertainty in the accumulated precipitation at 80 min are the aerosol concentration and the collection efficiency, and not the graupel aerodynamic parameter or the graupel density (the sweeping volume) which most influence the uncertainty in the maximum precipitation rate. Figure 6a shows that given the full uncertainty across all input parameters, the uncertainty in the collection efficiency of drops by graupel is by far the largest contributor to the output uncertainty for the accumulated precipitation at 80 min, with the Aitken and accumulation mode aerosol concentration providing a secondary source of uncertainty. However, the contributing sources change in the different regimes. Under the low aerosol conditions in regimes R1 and R3 (Figures 6b and 6d), the collection efficiency of the drops by graupel particles still dominates the output uncertainty, but the contribution from the aerosol parameter is reduced from that seen with respect to the full parameter space in Figure 6a. In contrast, under the high aerosol conditions in regimes R2 and R4 (Figures 6c and 6e), the concentration of the Aitken and accumulation mode aerosol provides a substantially larger contribution than the collection efficiency. We also see in Figures 6b and 6d that further input parameters make smaller contributions to the uncertainty in the accumulated precipitation at 80 min within the low aerosol regimes (R1 and R3) that were not seen to be important over the full parameter uncertainty space. In particular, the two primary freezing modes represented by the immersion freezing coefficient and the deposition freezing coefficient show more influence within regimes R3 and R1, respectively. Under low aerosol conditions, the warm rain process is not as suppressed as in the high aerosol cases. Some large drops freeze and become graupel particles which melt after falling down below the 0°C level and turn into rain.

Figure 8 shows the contributions to the uncertainty in the precipitation responses as box-whisker plots. The box part represents the median and interquartile range of the simulated distribution and the whisker extends to the distribution extremes (minimum and maximum values). The "All" column in each plot shows the overall uncertainty in the cloud precipitation response that is due to the joint parametric uncertainty from all of the input parameters together. The high collection efficiency regimes (R3 and R4) show much more overall variability in the precipitation responses than for the low collection efficiency regimes (R1 and R2). Also, the overall uncertainty distributions across the regimes for the maximum precipitation rate response are positively skewed, with long upper tails, whereas we see much more symmetric uncertainty distributions across the regimes for the accumulated precipitation response (with the exception of regime R2 which has a very strong positive skew).

The remaining columns in Figure 8 show box plot representations of the main effect contributions to the output uncertainty from each of the uncertain input parameters in turn, where the colors are as defined for the different regimes in section 4.1 and Figure 3. For each input parameter, the main effect index is essentially a scaled version of the individual variance contribution $V_i = \mathrm{Var}_{X_i}\{E_{\mathbf{X}_{-i}}[Y|X_i]\}$ to the overall decomposition of variance for the model output given by equation (B1) in Appendix B, where the notation $\mathbf{X}_{-\mathbf{i}}$ represents the full set of input parameters excluding parameter X_i. The box and whisker plots here have been produced by evaluating the distribution of the conditional statistical expectation over which the individual variance contributions V_i are calculated, $E_{\mathbf{X}_{-i}}[Y|X_i]$, via simulation from the fitted emulator model. For each input parameter X_i, this expectation was computed for 500 equally spaced values over the range of the conditioning input X_i, where each of these calculations of the expectation was made using 10,000 simulations over the parameter space defined by $\mathbf{X}_{-\mathbf{i}}$ for the given value of X_i. These box and whisker plots provide an indication of the variability in the precipitation response that is induced by the evaluated uncertainty in the individual input parameters, and they show the relative range within the overall

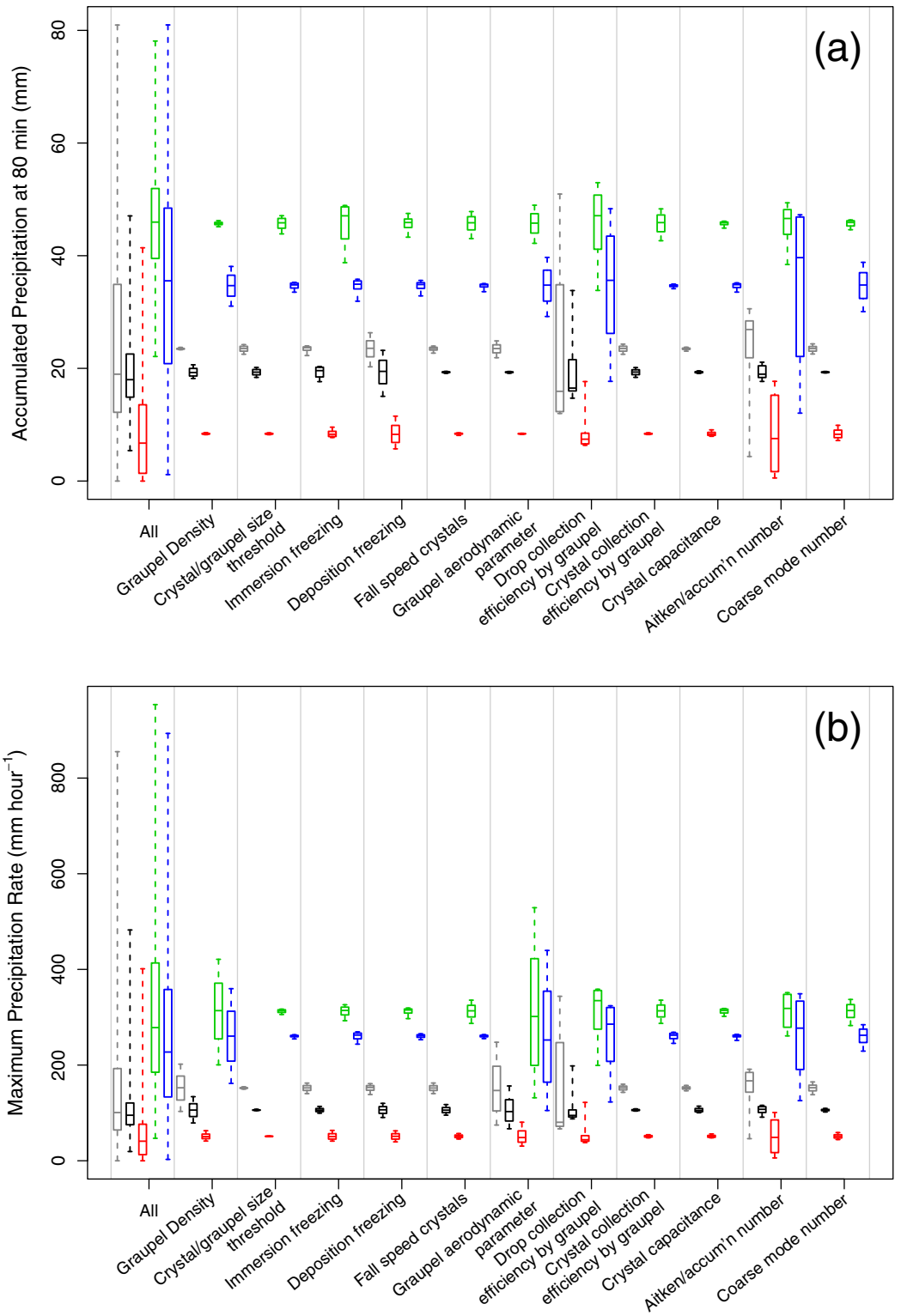

Figure 8. The individual contributions from each of the uncertain input parameters (*x* axis) to the uncertainty in (a) the accumulated precipitation at 80 min (Y_{11}), and (b) the maximum precipitation rate (Y_{12}), with respect to the full parameter uncertainty space (gray), and with respect to each of the different cloud regimes within this parameter space: R1 (black), R2 (red), R3 (green), and R4 (blue). The "All" columns show the overall uncertainty in these precipitation responses due to the parametric uncertainty in all inputs together.

uncertainty range of the output variable that each input parameter/regime acts. As for the overall uncertainty (shown by the "All" columns), we see greater variability in the output response of both the accumulated precipitation at 80 min and the maximum precipitation rate over the individual input contributions from the high collection efficiency regimes (R3 and R4). Finally, we note that Figure 8 also highlights the main input parameters that drive the parametric uncertainty in these precipitation responses across the different regimes and for the full parameter uncertainty space, and the conclusions here are as described above from Figure 6.

4.3.2. The Particle Responses

Figure 6 shows that the aerosol concentration parameter completely dominates the uncertainty in the drop number concentration in all cases (full parameter uncertainty and regimes) except one: in the high collection efficiency and low aerosol regime (R3) the collection efficiency of the drops by graupel particles shows a significantly larger contribution to the uncertainty than the aerosol parameter. This is because the depletion of drops by graupel particles can affect the number concentration of drops much more when aerosol (and therefore drop) concentrations are low, especially when the collection efficiency is high. In contrast, a range of input parameters contribute significantly to the uncertainty in the mean value of specific drop mass, but especially parameters that control the interaction between graupel particles and drops. Graupel particles affect the drop mass in two ways: they can decrease the drop mass by collecting drops and they can increase the drop mass through melting. Furthermore, the drops can freeze to become ice particles through the process of immersion freezing, which is a sink of drop mass. The uncertainty in the immersion freezing process (represented by the defined uncertainty in the immersion freezing coefficient) contributes significantly to the uncertainty in the drop mass for all cases in Figure 6. The concentration of the Aitken and accumulation modes of aerosol is also an important source, especially in the high aerosol regimes R2 and R4.

There are four main input parameters that lead to the uncertainty in the mean effective radius of the liquid drops. These are the parameters corresponding to the collection efficiency of drops by graupel particles, the graupel aerodynamic parameter, the graupel density and the concentration of the Aitken and accumulation mode aerosol. Each of these parameters contributes to the uncertainty in this model output by a similar amount for the analysis of the full parameter space (Figure 6a), but the contributions differ significantly across the regimes (Figures 6b–6e). In the early stages of the cloud development, the drop sizes are controlled by the warm rain process. However, in the later stages the melting of graupel particles produces large raindrops, affecting the mean effective radius of the drops (Figure 4). For the high aerosol but low collection efficiency regime (R2), the concentration of Aitken and accumulation mode aerosol contributes significantly to this output uncertainty, whereas for the high collection efficiency regimes and the low aerosol regimes (R1, R3 and R4) this is not the case. Here the inputs that relate to the properties of the graupel particles are the dominant sources.

For the mean graupel number concentration it is the threshold size at which particles are classed as graupel rather than ice crystals and the collection efficiency of drops by graupel that are the most significant sources to the parametric uncertainty in this model output. These two sources contribute by similar amounts when we consider the full parameter space, but within the defined regimes we see that the contribution from the threshold parameter is much greater for Regimes R1, R2, and R3. However, the reverse is true for regime R4 (high aerosol and high collection efficiency), which shows a much greater contribution from the collection efficiency. The dominating uncertainty source is different for regime R4 because the median radius of drops is small and less graupel particles form through primary freezing. Here interaction between ice and drops is a source of graupel formation. In all cases (the full parameter uncertainty space, and all regimes within this space), the immersion freezing coefficient and the concentration of the Aitken and accumulation mode aerosol provide small but still significant secondary contributions to the uncertainty in the mean number concentration of graupel particles.

The parametric uncertainty in the mean value of specific graupel mass is controlled by different uncertainty sources depending on the aerosol concentration. For the high aerosol regimes (R2 and R4), Figure 6 shows that the main contributor to the uncertainty is the concentration of the Aitken and accumulation modes of aerosol. This seems sensible as the more aerosol there is present, the more drops that can be formed and hence the more drops that can be collected by the graupel as they fall through the cloud, which in turn increases the average mass of the graupel particles. However it is the input parameters that control how

powerful (via the sweeping volume) and how efficiently the graupel particles collect the drops that mainly affect the output uncertainty for the low aerosol regimes (R1 and R3), since here the available drops are low in concentration. Hence, the uncertainty in the graupel aerodynamic parameter, the graupel density and the collection efficiency of the drops by graupel all make significant contributions to the uncertainty in the mean value of the graupel mass, along with the aerosol concentration, for these regimes. Finally, when we consider the full uncertainty across all of the input parameters together (Figure 6a), we see that it is the high aerosol regime behavior that dominates the uncertainty overall, with by far the largest contributor being the aerosol concentration parameter.

The input parameters driving the output uncertainty in the mean value of specific mass of ice crystals and the mean number concentration of ice crystals are very different to those driving the uncertainty for the mass and number concentration of the other particle types. For the number concentration of ice crystals, it is the uncertainty in the immersion freezing coefficient, the deposition freezing coefficient, the parameter describing the capacitance of ice crystals and the concentration of the Aitken and accumulation mode aerosol that provide the larger main effect contributions. Figure 6 shows that interaction effects account for 30–50% of the uncertainty in the mean ice crystal number concentration over the different analyses (full parameter uncertainty space and the four regimes), which is significantly more than for any of the other cloud responses considered. Much of this interaction is associated with the immersion freezing coefficient, the capacitance parameter and the aerosol concentration parameter (not shown in Figure 6).

For the mean value of specific ice crystal mass, the larger sources of uncertainty are related to the primary freezing modes: immersion freezing and deposition freezing, as well as the threshold that defines a particle as either ice crystal or graupel and the capacitance. For the high aerosol regimes, the immersion freezing coefficient is by far the dominating source of uncertainty. However, the threshold parameter is most significant for regime R1 (low aerosol and low collection efficiency), and in regime R3 (low aerosol and high collection efficiency) it is the capacitance that is the major contributor. These results indicate that the diffusional growth of ice crystals is sensitive to the different inputs in different ways, given the different conditions across the regimes.

4.3.3. The Cloud Dynamical Responses

Examining the responses that correspond to the cloud dynamics: the mean updraught and the mean downdraught, Figure 6a shows that overall (when we consider the whole parameter uncertainty space), the concentration of Aitken and accumulation mode aerosol is the main driver of the output uncertainty for both of these cloud responses. The remaining smaller contributions to the output uncertainty here are associated with the ice-phase latent heat release through immersion freezing, deposition freezing, capacitance, and the collection efficiency of drops by graupel. These dynamical responses are mainly driven by buoyancy in convective clouds. As cloud drops form and change phase (vapor to liquid, or liquid to ice), latent heat is released which can cause an increase in the mean updraught in the cloud. Conversely, cloud drops evaporating can cause a cooling effect, which can lead to an increase in the mean downdraught.

Exploring these model sensitivities further with respect to each of our defined regimes (Figures 6b–6e), we have found that the dominant contributor to the uncertainty in the mean updraught in the high aerosol regimes (R2 and R4), accounting for more than 80% of the output uncertainty, is the concentration of the Aitken and accumulation mode aerosol. In this regime, very high aerosol and drop concentrations lead to significant evaporative loss of drops in the ascending cloud parcels. In the low aerosol regimes (R1 and R3), the processes of the latent heat release in the ice-phase are the main sources, which controls the cloud buoyancy. These parameters are associated with the phase change from liquid to ice (immersion freezing and riming) and from vapor to ice (deposition freezing and the capacitance).

For the mean downdraught, we see that the aerosol concentration is the largest source of uncertainty for the high aerosol regimes R2 and R4, with the collection efficiency of drops by graupel providing an equivalent sized uncertainty source for regime R4 where this collection efficiency is defined to be high. For the low aerosol conditions (regimes R1 and R3) we see that the graupel aerodynamic parameter is the largest contributory source in regime R1, while the collection efficiency of drops by graupel takes over in regime R3, again where this collection efficiency is defined to be high. The graupel aerodynamic parameter and the collection efficiency affect the riming rate and hence the graupel mass, which is the water load related to downdraught.

Finally, we examine the uncertainty in the mean reflectivity. The reflectivity is related to the number of drops per unit volume and the sixth power of the drop diameter. Given the full parameter uncertainty space, Figure 6a indicates that the parametric uncertainty in the mean reflectivity is mainly due to the uncertainty in the collection efficiency of the drops by graupel particles and the concentration of the Aitken and accumulation modes of aerosol. There is also a small contribution from the uncertainty in the terminal fall speed of the graupel particles due to the aerodynamic parameter. However, considering the mean reflectivity individually for each of the defined regimes (Figures 6b–6e), we find that different inputs can dominate the uncertainty in this cloud response. In the low aerosol and low collection efficiency regime (R1), the collection efficiency of drops by graupel particles is the largest source, accounting for approximately 55% of the output uncertainty here. The second and the third sources of uncertainty are the graupel aerodynamic parameter and the graupel density. In the high aerosol regimes (R2 and R4), the aerosol concentration is the largest source, followed by the collection efficiency of drops by graupel particles. In the low aerosol and high collection efficiency regime (R3), the main sources are the graupel aerodynamic parameter, the collection efficiency of drops by graupel particles, and the graupel density.

Our analysis of Figure 6 also highlights that the uncertainty in each of the following input parameters: the terminal fall speed for ice crystals, the collection efficiency of ice crystals by graupel and the concentration of coarse mode aerosol, shows no real significant effect on the uncertainty in any of the twelve cloud responses that we consider here. This suggests that these parameters could easily be fixed within the MAC3 model at reasonable values with no real effect on the resulting model output.

Previous studies on sensitivity or uncertainty of cloud microphysics have used different methods, cloud conditions, or parameters. It has been found that even a small change in a parameter can cause big changes in the output [e.g., *Posselt and Vukicevic*, 2010; *Gilmore et al*., 2004]. Therefore, it is not feasible to make direct comparisons with other studies here. However, the results in this paper are in general agreement with the previous studies. For example, in the response of precipitation to aerosol [*Rosenfeld et al*., 2008; *Koren et al*., 2008], the impact of the collection efficiency by graupel [*Lillo and Mansell*, 2012], the impact of graupel density [*Gilmore et al*., 2004; *Milbrandt and Morrison*, 2013] and the impact of graupel terminal fall speeds [*McCumber et al*., 1991; *Hong et al*., 2009; *Van Weverberg et al*., 2013].

5. Summary and Discussion

We have identified the input parameters and model processes that drive output uncertainty in the simulation of a deep convective cloud for a selection of cloud responses. A set of 11 model input parameters from the MAC3 model were chosen to represent the main microphysical processes acting on the formation of a deep convective cloud, covering the initial formation of drops and ice crystals, the diffusional growth of ice particles, and the interactions between cloud particles. The uncertainties of the input parameters were assessed through an expert elicitation exercise using literature information and knowledge of the capabilities and assumptions in the model. These parameter ranges then formed the 11 dimensional parameter uncertainty space over which the uncertainty in each cloud response was evaluated using the statistical tools of experiment design, Gaussian process emulation and variance-based sensitivity analysis.

The analysis highlighted four distinct cloud behaviors (regimes) within the parameter uncertainty space, defined by the Aitken and accumulation mode aerosol concentrations and the collection efficiency of drops by graupel. These regimes showed visible differences in the simulated cloud, with different input factors controlling the parametric uncertainty.

Across all cloud responses, the uncertain inputs that have the greatest influence on the model uncertainty are the concentrations of Aitken and accumulation mode particles and the collection efficiency of cloud drops by graupel particles. However, the drivers of the parametric uncertainty within the four regimes can be very different in comparison to when we consider the full parameter uncertainty space (all regimes together). In particular, it is the uncertainty contributions from parameters that represent the primary freezing modes and the properties and the behavior of graupel particles in the model that correspond to many of these differences.

The largest overall contributor to output uncertainty is the concentration of Aitken and accumulation mode aerosol. This parameter influences the uncertainty in every model output. However, the role of the Aitken and accumulation mode aerosol becomes secondary in low aerosol regimes (Aitken and accumulation

mode particle concentrations less than 1600 cm^{-3}) where the collection efficiency of drops by graupel is the most important factor. The coarse mode of aerosol shows very little effect on the uncertainty in the model outputs, except at very high aerosol concentrations, when it affects the effective radius, the drop mass, and the accumulated precipitation.

The collection efficiency of drops by graupel is the second biggest contributor overall to output uncertainty, and the largest contributor when the aerosol concentration is low and the collection of drops by graupel is strong. This parameter affects the accumulated precipitation, the maximum precipitation rate, the drop mass and concentration, the graupel mass and concentration, the updraught and downdraught, the effective radius and the reflectivity. Hence, it is a very important model parameter for cloud dynamics, cloud microphysics and precipitation responses. In contrast, the collection efficiency of ice crystals by graupel is a relatively unimportant parameter for model uncertainty.

The immersion freezing coefficient is the third largest overall contributor to the parametric model uncertainty. Uncertainty in this parameter is important for the ice crystal mass and number concentration, the drop mass, the graupel number concentration, and the updraught. The deposition freezing coefficient plays a much less significant role in the simulated deep cloud, but this result may be different for shallow clouds.

The input parameters that represent properties of the ice crystals have a much smaller effect on the parametric uncertainty in comparison to those representing the graupel particles. However, the capacitance (shape) of ice crystals still shows some small but significant contributions to the uncertainty in the ice crystal mass and number concentration, as well as the updraught and downdraught, especially for the low aerosol regimes. Although parameters related to ice crystals are not as important to precipitation as those associated with graupel particles, they are likely to be more important with respect to atmospheric radiation. Given the large multimodel diversity in ice water path [*Waliser et al*., 2009], improvements in such ice processes would be valuable.

Our analysis reveals that parameters related to particle properties and interactions contribute more to model uncertainty than the initial aerosol loading. Reducing uncertainty with respect to the interaction between graupel particles and drops provides both challenges and opportunities for laboratory experiments, theoretical studies and modeling in order to improve simulations of precipitation. Three uncertain parameters that we consider in this work can affect the interaction between graupel particles and drops. These are the graupel density, the graupel aerodynamic parameter, and the collection efficiency of drops by graupel. The uncertainty in these parameters feeds through the model to have very different effects on the uncertainty in the two precipitation properties we consider. For example, the graupel aerodynamic parameter has been shown to contribute significantly to the uncertainty in the maximum precipitation rate but has very little effect on the uncertainty in the accumulated precipitation.

The information obtained in this study could be used for improving other models. For liquid drops, a good representation of activated cloud condensation nuclei and the collection processes are important. For example, *Kogan* [2013] developed a new scheme with the help of bin-resolved microphysics to improve the autoconversion rate. The improvement in other processes, such as the collections by graupel, can be achieved similarly by using models with bin-resolved microphysics.

In addition to the parametric uncertainty that we have explored here, we acknowledge that cloud models are subject to other forms of uncertainty. These include structural uncertainty with respect to how the cloud microphysics and processes are defined and implemented, and the discrepancy between the model and the real world system it aims to represent. We also recognize that we have only simulated a single deep convective cloud in a continental environment. Our previous study [*Cui et al*., 2011a] indicates that the nature of continental cloud response is generally the same for a wide range of aerosol and thermodynamic conditions at various locations, suggesting that the conclusions of our uncertainty analysis should apply to deep convective clouds in other continental environments. However, the conclusions could be different for other cloud types, such as deep convective clouds over the ocean, shallow cumulus clouds or cumulus congestus clouds. Finally, we note that systems of interacting clouds (or cloud fields) often behave very differently to individual cloud cells. Our understanding of key uncertainties in how cloud systems depend on environmental conditions and microphysical parameters could be greatly advanced by extending the emulator approach used here.

Appendix A: Gaussian Process Emulation

Through the application of Gaussian process emulation to the cloud microphysics model MAC3 we are able to evaluate the MAC3 model outputs across all dimensions of the defined parameter uncertainty space simultaneously and assess the model sensitivity using variance-based sensitivity analysis—tasks that would not be possible with the cloud model simulator alone due to the computational complexity and substantial run time of the model. The Gaussian process emulator is defined by the following statistical theory:

Let the function $\eta(\cdot)$ represent an aspect of a model simulator such that a model output of interest Y can be predicted from a set of d uncertain input parameters $\mathbf{X}=\{X_1, X_2, \ldots, X_d\}$, defined over a d-dimensional parameter uncertainty space through the relation $Y=\eta(\mathbf{X})$. An emulator for $\eta(\cdot)$ to predict Y is constructed by combining a set of runs from the model simulator (training data) with prior beliefs about the behavior of the model using a Bayesian statistical approach. Here the Gaussian process is used to represent our beliefs about the model behavior. The Gaussian process is a generalization of the multivariate Gaussian distribution to infinitely many variables, and any finite set of random variables from this process also follows a Gaussian distribution. The Gaussian process is defined in terms of two elements: a mean function and a covariance structure. Letting $\boldsymbol{x}=\{x_1, x_2, \ldots, x_d\}$ denote a given realization of $\mathbf{X}$, a priori we represent our beliefs about the model behavior as a d-dimensional Gaussian process such that:

$$\eta(\boldsymbol{x}) \sim \mathcal{GP}[m(\boldsymbol{x}), V(\boldsymbol{x}, \boldsymbol{x}')], \tag{A1}$$

where $m(\boldsymbol{x})$ and $V(\boldsymbol{x}, \boldsymbol{x}')$ correspond to the mean and covariance functions of the Gaussian process, respectively. This prior specification is updated using the training data from the model simulator to obtain a conditional posterior distribution for $\eta(\cdot)$ in terms of an updated mean and covariance structure—a conditional Gaussian process given the information from the training data. This posterior specification is the emulator, where the mean function is used to estimate the model output Y, and the corresponding covariance structure provides an estimate of uncertainty for this mean function prediction.

To construct the prior Gaussian process, the form of $m(\cdot)$ and $V(\cdot, \cdot)$ in equation (A1) must be specified. Typically the mean function is given by:

$$m(\boldsymbol{x})=E[\eta(\boldsymbol{x})|\boldsymbol{\beta}]=\mathbf{h}(\boldsymbol{x})^T\boldsymbol{\beta},$$

where $\mathbf{h}(\cdot)$ is a vector of known regression functions of $\boldsymbol{x}$ and $\boldsymbol{\beta}$ is a corresponding vector of unknown regression coefficients. The structure of $\mathbf{h}(\cdot)$ is chosen to reflect any beliefs about the form of $\eta(\cdot)$. The covariance function $V(\cdot, \cdot)$ specifies the covariance in the output Y for any pair of parameter input combinations $\boldsymbol{x}$ and $\boldsymbol{x}'$, and is given by:

$$V(\boldsymbol{x}, \boldsymbol{x}')=\mathrm{cov}(\eta(\boldsymbol{x}), \eta(\boldsymbol{x}')|\sigma^2)=\sigma^2 k(\boldsymbol{x}, \boldsymbol{x}'|\boldsymbol{\psi}).$$

Here the function $k(\boldsymbol{x}, \boldsymbol{x}'|\boldsymbol{\psi})$ is a given correlation function with unknown hyperparameters $\boldsymbol{\psi}=(\psi_1, \psi_2, \ldots, \psi_d)$ that represent the smoothness of the model response to the uncertain input parameters, and σ^2 is an unknown scale parameter. Using the Gaussian process means that the modeled surface of the output Y over the parameter uncertainty space is assumed to be *smooth* and the emulator will break down if this assumption is violated (e.g., if there are discontinuities in the modeled output or the output is chaotic). The correlation function $k(\boldsymbol{x}, \boldsymbol{x}'|\boldsymbol{\psi})$ is defined to be stationary (as the distance between any two inputs $|\boldsymbol{x}-\boldsymbol{x}'|$ within the parameter space increases the correlation value decreases), positive semidefinite, and $k(\boldsymbol{x}, \boldsymbol{x})=1$ for all $\boldsymbol{x}$. *Rasmussen and Williams* [2006] outline a selection of different structures for the form of $k(\boldsymbol{x}, \boldsymbol{x}'|\boldsymbol{\psi})$, with the most commonly used being the very smooth squared exponential (Gaussian) form and the Matérn form. The Matérn structure is chosen for the emulator fits in this study as this form copes better with any slight roughnesses in the model output surface, which could potentially occur to a small degree in outputs from a complex cloud microphysics model. Each of the unknown hyperparameters $\boldsymbol{\beta}, \sigma^2$ and $\boldsymbol{\psi}$ of the covariance function $V(\cdot, \cdot)$ can be varied to adjust the behavior and fit of an emulator. It is very difficult to specify any kind of prior specification on these model hyperparameters in advance of the model fitting procedure, and therefore weak conjugate prior distributions are assumed over them in the Bayesian analysis. This means that no real information on Y is contributed to the emulator from any prior specifications and that these hyperparameters are essentially estimated from the training data. A popular method to estimate the

values of these parameters to produce a reasonable fit of the emulator is to maximize the marginal likelihood function, as described in *Rasmussen and Williams* [2006].

Training data for an emulator are obtained by running a set of n input combinations $\mathbf{x}=\{\boldsymbol{x_1}, \boldsymbol{x_2}, \ldots, \boldsymbol{x_n}\}$ through the model simulator to obtain the corresponding model outputs $\boldsymbol{y}=\{y_1, y_2, \ldots, y_n\}$. These n input combinations are selected using a space-filling design algorithm over the parameter uncertainty space, such as the maximin Latin hypercube design [*Morris and Mitchell*, 1995]. By selecting the training data in this way, optimal information about the behavior of the model output Y over the parameter uncertainty space is obtained from it to inform any predictions for Y from the emulator. The number of training runs to use (n) is also an unknown here. The value of n can depend on the number of active input parameters and the function smoothness, but in general a "rule of thumb" to use $n=10d$ runs is applied [*Loeppky et al.*, 2009], where d is the number of uncertain input parameters over which the emulator is to be built.

Via the Bayesian paradigm, the Gaussian process prior specification in equation (A1) is updated using the training data to obtain a posterior specification that takes the form of a Student t-process (a Gaussian process with estimated variance) with $n - q$ degrees of freedom, where q is the number or elements in $\boldsymbol{\beta}$, derived from the prior choice of $\mathbf{h}(\cdot)$. The mean function of this posterior process is given by:

$$m^*(\boldsymbol{x})=\mathbf{h}(\boldsymbol{x})^T\hat{\beta}+\mathbf{t}(\boldsymbol{x})^T A^{-1}(\boldsymbol{y}-\mathbf{H}\hat{\beta}),$$

and the posterior covariance function is:

$$\begin{aligned} V^*(\boldsymbol{x},\boldsymbol{x}')&=\hat{\sigma}^2 k^*(\boldsymbol{x},\boldsymbol{x}') \\ &=\hat{\sigma}^2[k(\boldsymbol{x},\boldsymbol{x}'|\boldsymbol{\psi})-\mathbf{t}(\boldsymbol{x})^T A^{-1}\mathbf{t}(\boldsymbol{x}') \\ &+(\mathbf{h}(\boldsymbol{x})^T-\mathbf{t}(\boldsymbol{x})^T A^{-1}\mathbf{H})(\mathbf{H}^T A^{-1}\mathbf{H})^{-1}(\mathbf{h}(\boldsymbol{x}')^T-\mathbf{t}(\boldsymbol{x}')^T A^{-1}\mathbf{H})^T], \end{aligned} \tag{A2}$$

where

$$\mathbf{t}(\boldsymbol{x})^T=(k(\boldsymbol{x},\boldsymbol{x_1}),\ldots,k(\boldsymbol{x},\boldsymbol{x_n})), \mathbf{H}^T=(\mathbf{h}(\boldsymbol{x_1}),\ldots,\mathbf{h}(\boldsymbol{x_n})),$$

$$A=, \begin{pmatrix} 1 & k(\boldsymbol{x_1},\boldsymbol{x_2}) & \cdots & k(\boldsymbol{x_1},\boldsymbol{x_n}) \\ k(\boldsymbol{x_2},\boldsymbol{x_1}) & 1 & & \vdots \\ \vdots & & \ddots & \\ k(\boldsymbol{x_n},\boldsymbol{x_1}) & \cdots & & 1 \end{pmatrix}$$

$$\hat{\beta}=(\mathbf{H}^T A^{-1}\mathbf{H})^{-1}\mathbf{H}^T A^{-1}\mathbf{y},$$

and

$$\hat{\sigma}^2=\frac{\mathbf{y}^T(A^{-1}-A^{-1}\mathbf{H}(\mathbf{H}^T A^{-1}\mathbf{H})^{-1}\mathbf{H}^T A^{-1})\mathbf{y}}{n-q-2}.$$

This posterior process is the fitted emulator for $Y=\eta(\mathbf{X})$. A full derivation of this result can be found in *O'Hagan* [1994].

The final stage in the construction of the emulator is the process of validation. Validation of an emulator is important as there is no guarantee that the training data used to build the emulator are sufficient to describe the output of interest Y at other locations $\boldsymbol{x} \notin \mathbf{x}$ within the parameter uncertainty space. *Bastos and O'Hagan* [2009] describe a range of methods for emulator validation. Once validated, the emulator can be used to predict the output $y=\eta(\boldsymbol{x})$ at any point $\boldsymbol{x}$ in the parameter uncertainty space, along with a measure of uncertainty in that prediction, using the given formulae.

Appendix B: Variance-Based Sensitivity Analysis

Variance-based sensitivity analysis is a statistical technique by which the overall variance for an output Y can be decomposed into its contribution sources. This statistical tool can help us to explore and understand the behavior of a complex model, establish how different parts of the model interplay and determine the uncertain input factors that most influence the uncertainty in an output variable. *Saltelli et al.* [2000] provide a detailed overview of variance-based methods for sensitivity analysis. In this study, we implement the extended FAST (Fourier Amplitude Sensitivity Test) approach of *Saltelli et al.* [1999] to compute our sensitivity measures.

For a given set of independent model input parameters $\boldsymbol{X}=\{X_1, X_2, \ldots, X_d\}$ defined over a d-dimensional parameter uncertainty space, and an output variable of interest Y, the variance in the prediction for Y due to the uncertainty in $\mathbf{X}$, $V=\mathrm{Var}\{E[Y|\boldsymbol{X}]\}$, can be decomposed into terms relating to contributions from individual parameters (main effects) and contributions from parameter interactions. Let the notation: $V_i=\mathrm{Var}_{X_i}\{E_{\boldsymbol{X}_{-i}}[Y|X_i]\}$ represent the expected amount by which the uncertainty in the model output Y will be reduced if the input parameter X_i were known exactly, where $\boldsymbol{X}_{-i}$ indicates the set of all input parameters in $\mathbf{X}$ except for X_i. Extending this, we have that the expected reduction in uncertainty if we were to learn two inputs X_i and X_j is given by $V_{i,j}=\mathrm{Var}_{X_{ij}}\{E_{\boldsymbol{X}_{-ij}}[Y|\boldsymbol{X}_{i,j}]\}=V_i+V_j+W_{i,j}$. Here $W_{i,j}$ is an extra amount of variance over the individual contributions from these inputs that is removed, corresponding solely to uncertainty about the interaction between the inputs X_i and X_j. By considering the uncertainty due to larger sets of inputs together, higher order interaction terms can be isolated. Hence, it follows that the uncertainty in Y can be represented as a decomposition into variance contributions from both individual inputs and interaction terms [*Oakley and O'Hagan*, 2004], given by:

$$V=\mathrm{Var}\{E[Y|\boldsymbol{X}]\}=\sum_{i=1}^{d} V_i+\sum_{i<j} W_{i,j}+\sum_{i<j<k} W_{i,j,k}+\cdots+W_{1,2,\ldots,d}. \tag{B1}$$

The sensitivity measures that we consider are the main effect index and the total effect index, which are derived directly from the components of the variance decomposition in equation (B1). The main effect index for input parameter X_i, also described as the first order sensitivity index for X_i, is defined as:

$$S_i=\frac{V_i}{V}, \tag{B2}$$

and is a measure of the fractional contribution of X_i to the variance of Y. For $i \neq j$, the second order sensitivity index $S_{i,j}=W_{i,j}/V$ represents the interaction effect due to X_i and X_j. This corresponds to a measure of the extra uncertainty in Y due to X_i and X_j that cannot be explained by the individual main effect contributions S_i and S_j alone. Higher order sensitivity indices representing higher order interactions are defined in a similar way. These sensitivity indices have the property that

$$\sum_{i=1}^{d} S_i+\sum_{i<j} S_{i,j}+\cdots+S_{1,2,\ldots,d}=1. \tag{B3}$$

The total effect index for input parameter X_i, S_{T_i}, is defined as the sum of all sensitivity indices within the left-hand side of equation (B3) that involve X_i. This can also be defined as:

$$S_{T_i}=\frac{V_{T_i}}{V}, \tag{B4}$$

where V_{T_i} represents all variance components in equation (B1) that include X_i. If input X_i has no interactions with any other input parameters, then $S_i=S_{T_i}$. The value of the difference $S_{T_i}-S_i$ provides an indication of how much input X_i is interacting with the other input parameters and allows the sensitivity of the model output Y to interactions to be assessed.

Given these two defined sensitivity measures, the main parameters (and therefore model processes and mechanisms) that lead to the parametric uncertainty in model outputs of interest can be evaluated.

Acknowledgments

The data used and generated in this work can be made available upon request from the corresponding author (J.S.Johnson@leeds.ac.uk). This work was supported by the Natural Environment Research Council ACID-PRUF project under grant NE/I020059/1 and GASSP project under grant NE/J024252/1. K. S. Carslaw is currently a Royal Society Wolfson Merit Award holder.

References

Adams-Selin, R. D., S. C. van den Heever, and R. H. Johnson (2013), Sensitivity of bow-echo simulation to microphysical parameterizations, *Weather Forecasting*, *28*, 1188–1209, doi:10.1175/WAF-D-12–00108.1.

Bailey, M., and J. Hallett (2012), Ice crystal linear growth rates from −20°C to −70°C: Confirmation from wave cloud studies, *J. Atmos. Sci.*, *69*, 390–402, doi:10.1175/JAS-D-11–035.1.

Bastos, L. S., and A. O'Hagan (2009), Diagnostics for Gaussian process emulators, *Technometrics*, *51*(4), 425–438, doi:10.1198/TECH.2009.08019.

Blyth, A. M., J. H. Lowenstein, Y. Huang, Z. Cui, S. Davies, and K. S. Carslaw (2013), The production of warm rain in shallow maritime cumulus clouds, *Q. J. R. Meteorol. Soc.*, *139*, 20–31, doi:10.1002/qj.1972.

Böhm, H. P. (1989), A general equation for the terminal fall speed of solid hydrometeors, *J. Atmos. Sci.*, *46*, 2419–2427, doi:10.1175/1520-0469(1989)046<2419:AGEFTT>2.0.CO;2.

Boucher, O., et al. (2013), Clouds and aerosols, in *Climate Change 2013: The Physical Science Basis. Contribution of Working Group I to the Fifth Assessment Report of the Intergovernmental Panel on Climate Change*, 571–657, edited by T. F. Stocker, et al., Cambridge Univ. Press, Cambridge, U. K.

Cotton, W. R., G. H. Bryan, and S. C. van den Heever (2011), *Storm and Cloud Dynamics, Int. Geophys. Ser.*, 2nd ed., vol. 99, Academic, Burlington, Mass.
Cui, Z., and K. S. Carslaw (2006), Enhanced vertical transport efficiency of aerosol in convective clouds due to increases in tropospheric aerosol abundance, *J. Geophys. Res.*, *111*, D15212, doi:10.1029/2005JD006781.
Cui, Z., K. S. Carslaw, Y. Yin, and S. Davies (2006), A numerical study of aerosol effects on the dynamics and microphysics of a deep convective cloud in a continental environment, *J. Geophys. Res.*, *111*, D05201, doi:10.1029/2005JD005981.
Cui, Z., S. Davies, K. S. Carslaw, and A. M. Blyth (2011a), The response of precipitation to aerosol through riming and melting in deep convective clouds, *Atmos. Chem. Phys.*, *11*, 3495–3510, doi:10.5194/acp-11-3495-2011.
Cui, Z., K. S. Carslaw, and A. M. Blyth (2011b), The coupled effect of mid-tropospheric moisture and aerosol abundance on deep convective cloud dynamics and microphysics, *Atmosphere*, *2*, 222–241, doi:10.3390/atmos2030222.
Dearden, C., P. J. Connolly, T. W. Choularton, and P. R. Field (2011), Evaluating the effects of microphysical complexity in idealised simulations of trade wind cumulus using the factorial method, *Atmos. Chem. Phys.*, *11*, 2729–2746, doi:10.5194/acp-11-2729-2011.
Diehl, K., and S. Wurzler (2004), Heterogeneous drop freezing in the immersion mode: Model calculations considering soluble and insoluble particles in the drops, *J. Atmos. Sci.*, *61*, 2063–2072, doi:10.1175/1520-0469(2004)061<2063:HDFITI>2.0.CO;2.
Gilmore, M. S., J. M. Straka, and E. N. Rasmussen (2004), Precipitation uncertainty due to variations in precipitation particle parameters within a simple microphysics scheme, *Mon. Weather Rev.*, *132*, 2610–2627, doi:10.1175/MWR2810.1.
Guo, Z., M. Wang, Y. Qian, V. E. Larson, S. Ghan, M. Ovchinnikov, P. A. Bogenschutz, C. Zhao, G. Lin, and T. Zhou (2014), A sensitivity analysis of cloud properties to CLUBB parameters in the single-column Community Atmosphere Model (SCAM5), *J. Adv. Model. Earth Syst.*, *6*, 829–858, doi:10.1002/2014MS000315.
Heymsfield, A., and R. Wright (2014), Graupel and hail terminal velocities: Does a "Supercritical" Reynolds number apply?, *J. Atmos. Sci.*, *71*, 3392–3403, doi:10.1175/JAS-D-14-0034.1.
Hobbs, P. V., D. A. Bowdle, and L. F. Radke (1985), Particles in the lower troposphere over the high plains of the United States. Part I: Size distributions, elemental composition and morphologies, *J. Clim. Appl. Meteorol.*, *24*, 1344–1356, doi:10.1175/1520-0450(1985)024<1344:PITLTO>2.0.CO;2.
Hong, S., K. Sunny Lim, J. Kim, J. Lim, and J. Dudhia (2009), Sensitivity study of cloud-resolving convective simulations with WRF using two bulk microphysical parameterizations: Ice-phase microphysics versus sedimentation effects, *J. Appl. Meteorol. Climatol.*, *48*, 61–76, doi:10.1175/2008JAMC1960.1.
Huang, Y., A. M. Blyth, P. R. A. Brown, T. W. Choularton, P. Connolly, A. M. Gadian, H. Jones, J. Latham, Z. Cui, and K. Carslaw (2008), The development of ice in a cumulus cloud over southwest England, *New J. Phys.*, *10*, 105021, doi:10.1088/1367-2630/10/10/105021.
Kaufman, Y. J., I. Koren, L. A. Remer, D. Rosenfeld, and Y. Rudich (2005), The effect of smoke, dust, and pollution aerosol on shallow cloud development over the Atlantic Ocean, *Proc. Natl. Acad. Sci. U. S. A.*, *102*(32), 11,207–11,212, doi:10.1073/pnas.0505191102.
Kennedy, M. C., and A. O'Hagan (2001), Bayesian calibration of computer models, *J. R. Stat. Soc., Ser. B*, *63*(3), 425–464, doi:10.1111/1467-9868.00294.
Khain, A. P., M. Ovtchinnikov, M. Pinsky, A. Pokrovsky, and H. Krugliak (2000), Notes on the state-of-the-art numerical modeling of cloud microphysics, *Atmos. Res.*, *55*, 159–224, doi:10.1016/S0169-8095(00)00064-8.
Kogan, Y. (2013), A cumulus cloud microphysics parameterization for cloud-resolving models, *J. Atmos. Sci.*, *70*, 1423–1436, doi:10.1175/JAS-D-12–0183.1.
Koren, I., J. V. Martins, L. A. Remer, and H. Afargan (2008), Smoke invigoration versus inhibition of clouds over the Amazon, *Science*, *321*, 946–949, doi:10.1126/science.1159185.
Lamb, D., and J. Verlinde (2011), *Physics and Chemistry of Clouds*, Cambridge Univ. Press, Cambridge, U. K.
Lee, L. A., K. S. Carslaw, K. J. Pringle, G. W. Mann, and D. V. Spracklen (2011), Emulation of a complex global aerosol model to quantify sensitivity to uncertain parameters, *Atmos. Chem. Phys.*, *11*, 12,253–12,273, doi:10.5194/acp-11-12253-2011.
Lee, L. A., K. J. Pringle, C. L. Reddington, G. W. Mann, P. Stier, D. V. Spracklen, J. R. Pierce, and K. S. Carslaw (2013), The magnitude and causes of uncertainty in global model simulations of cloud condensation nuclei, *Atmos. Chem. Phys.*, *13*, 8879–8914, doi:10.5194/acp-13-8879-2013.
Lillo, S., and E. Mansell (2012), Sensitivity of microphysical parameters on the evolution of a supercell, paper presented at 92nd American Meteorological Society Annual Meeting, New Orleans, La., 22–26 Jan.
Locatelli, J. D., and P. V. Hobbs (1974), Fallspeeds and masses of solid precipitation particles, *J. Geophys. Res.*, *79*(15), 2185–2197, doi:10.1029/JC079i015p02185.
Loeppky, J. L., J. Sacks, and W. J. Welch (2009), Choosing the sample size of a computer experiment: A practical guide, *Technometrics*, *51*(4), 366–376, doi:10.1198/TECH.2009.08040.
McCumber, M., W.-K. Tao, J. Simpson, R. Penc, and S.-T. Soong (1991), Comparison of ice-phase microphysical parameterization schemes using numerical simulations of tropical convection, *J. Appl. Meteorol.*, *30*, 985–1004, doi:10.1175/1520-0450-30.7.985.
McDonald, J. E. (1963), Use of the electrostatic analogy in studies of ice crystal growth, *Z. Angew. Math. Phys.*, *14*, 610–620, doi:10.1007/BF01601268.
Meyers, M. P., P. J. DeMott, and W. R. Cotton (1992), New primary ice-nucleation parameterizations in an explicit cloud model, *J. Appl. Meteorol.*, *31*, 708–721, doi:10.1175/1520-0450(1992)031<0708:NPINPI>2.0.CO;2.
Milbrandt, J. A., and H. Morrison (2013), Prediction of graupel density in a bulk microphysics scheme, *J. Atmos. Sci.*, *70*, 410–429, doi:10.1175/JAS-D-12-0204.1.
Milbrandt, J. A., and M. K. Yau (2006), A multimoment bulk microphysics parameterization. Part IV: Sensitivity experiments, *J. Atmos. Sci.*, *63*, 3137–3159, doi:10.1175/JAS3817.1.
Mitchell, D. L., and A. J. Heymsfield (2005), Refinements in the treatment of ice particle terminal velocities, highlighting aggregates, *J. Atmos. Sci.*, *62*, 1637–1644, doi:10.1175/JAS3413.1.
Morris, M. D., and T. J. Mitchell (1995), Exploratory designs for computer experiments, *J. Stat. Plann. Inference*, *43*, 381–402, doi:10.1016/0378–3758(94)00035-T.
Morrison, H., and W. W. Grabowski (2007), Comparison of bulk and bin warm-rain microphysics models using a kinematic framework, *J. Atmos. Sci.*, *64*, 2839–2861, doi:10.1175/JAS3980.
Morrison, H., and J. Milbrandt (2015), Parameterization of cloud microphysics based on the prediction of bulk ice particle properties. Part 1: Scheme description and idealized tests, *J. Atmos. Sci.*, *72*, 287–311, doi:10.1175/JAS-D-14–0065.1.
Morrison, H., G. Thompson, and V. Tatarskii (2009), Impact of cloud microphysics on the development of trailing stratiform precipitation in a simulated squall line: Comparison of one- and two-moment schemes, *Mon. Weather Rev.*, *137*, 991–1007, doi:10.1175/2008MWR2556.1.

Murray, B. J., D. O'Sullivan, J. D. Atkinson, and M. E. Webb (2012), Ice nucleation by particles immersed in supercooled cloud droplets, *Chem. Soc. Rev.*, *41*, 6519–6554, doi:10.1039/c2cs35200a.

Oakley, J. E., and A. O'Hagan (2004), Probabilistic sensitivity analysis of complex models: A Bayesian approach, *J. R. Stat. Soc., Ser. B*, *66*, 751–69, doi:10.1111/j.1467–9868.2004.05304.x.

O'Hagan, A. (1978), Curve fitting and optimal design for prediction, *J. R. Stat. Soc., Ser. B*, *40*(1), 1–42.

O'Hagan, A. (1994), *Kendall's Advanced Theory of Statistics: Bayesian Inference*, vol. 2B, Edward Arnold, London, U. K.

O'Hagan, A. (2006), Bayesian analysis of computer code outputs: A tutorial, *Reliab. Eng. Syst. Safety*, *91*, 1290–1300, doi:10.1016/j.ress.2005.11.025.

O'Hagan, A., C. E. Buck, A. Daneshkhah, J. R. Eiser, P. H. Garthwaite, D. J. Jenkinson, J. E. Oakley, and T. Rakow (2006), *Uncertain Judgements: Eliciting Expert Probabilities*, John Wiley, Chichester, U. K.

Posselt, D. J., and T. Vukicevic (2010), Robust characterization of model physics uncertainty for simulations of deep moist convection, *Mon. Weather Rev.*, *138*, 1513–1535, doi:10.1175/2009MWR3094.1.

Pruppacher, H. R., and J. D. Klett (1997), *Microphysics of Clouds and Precipitation*, Kluwer Acad., Dordrecht, Netherlands.

Pujol, G., B. Iooss, and A. Janon (2013), *Sensitivity: Sensitivity Analysis, R Package Version 1.7*. [Available at http://CRAN.R-project.org/package=sensitivity.]

R Core Team (2013), *R: A Language and Environment for Statistical Computing*, R Found. for Stat. Comput., Vienna.

Rasmussen, C. E., and C. K. I. Williams (2006), *Gaussian Processes for Machine Learning*, MIT Press, London, U. K.

Reid, J. S., B. Brooks, K. K. Crahan, D. A. Hegg, T. F. Eck, N. O'Neill, G. de Leeuw, E. A. Reid, and K. D. Anderson (2006), Reconciliation of coarse mode sea-salt aerosol particle size measurements and parameterizations at a subtropical ocean receptor site, *J. Geophys. Res.*, *111*, D02202, doi:10.1029/2005JD006200.

Reisin, T., Z. Levin, and S. Tzivion (1996), Rain production in convective clouds as simulated in an axisymmetric model with detailed microphysics. Part I: Description of the model, *J. Atmos. Sci.*, *53*(3), 497–520, doi:10.1175/1520-0469(1996)053<0497:RPICCA>2.0.CO;2.

Respondek, P. S., A. I. Flossmann, R. R. Alheit, and H. R. Pruppacher (1995), A theoretical study of the wet removal of atmospheric pollutants. Part V: The uptake, redistribution, and deposition of $(NH_4)_2SO_4$ by a convective cloud containing ice., *J. Atmos. Sci.*, *52*, 2121–2132, doi:10.1175/1520-0469(1995)052<2121:ATSOTW>2.0.CO;2.

Rosenfeld, D., U. Lohmann, G. B. Raga, C. D. O'Dowd, M. Kulmala, S. Fuzzi, A. Reissell, and M. O. Andreae (2008), Flood or drought: How do aerosols affect precipitation?, *Science*, *321*, 1309–1313, doi:10.1126/science.1160606.

Rougier, J., D. M. H. Sexton, J. M. Murphy, and D. Stainforth (2009), Analyzing the climate sensitivity of the HadSM3 climate model using ensembles from different but related experiments, *J. Clim.*, *22*, 3540–3557, doi:10.1175/2008JCLI2533.1.

Roustant, O., D. Ginsbourger, and Y. Deville (2012), DiceKriging, DiceOptim: Two R packages for the analysis of computer experiments by kriging-based metamodeling and optimization, *J. Stat. Software*, *51*(1), 1–55.

Sacks, J., W. J. Welch, T. J. Mitchell, and H. P. Wynn (1989), Design and analysis of computer experiments, *Stat. Sci.*, *4*(4), 409–435, doi:10.1214/ss/1177012413.

Saltelli, A., S. Tarantola, and K. Chan (1999), A quantitative model-independent method for global sensitivity analysis of model output, *Technometrics*, *41*(1), 39–56, doi:10.1080/00401706.1999.10485594.

Saltelli, A., K. Chan, and E. M. Scott (2000), *Sensitivity Analysis*, John Wiley, N. Y.

Santner, T. J., B. J. Williams, and W. Notz (2003), *The Design and Analysis of Computer Experiments*, Springer, N. Y.

Tzivion, S., G. Feingold, and Z. Levin (1987), An efficient numerical solution to the stochastic collection equation, *J. Atmos. Sci.*, *44*(21), 3139–3149, doi:10.1175/1520-0469(1987)044<3139:AENSTT>2.0.CO;2.

Vali, G. (1985), Nucleation terminology, *J. Aerosol Sci.*, *16*, 575–576, doi:10.1016/0021–8502(85)90009-6.

Van Weverberg, K., A. M. Vogelmann, W. Lin, E. P. Luke, A. Cialella, P. Minnis, M. Khaiyer, E. R. Boer, and M. P. Jensen (2013), The role of cloud microphysics parameterization in the simulation of mesoscale convective system clouds and precipitation in the tropical western pacific, *J. Atmos. Sci.*, *70*, 1104–1128, doi:10.1175/JAS-D-12–0104.1.

von Blohn, N., K. Diehl, S. K. Mitra, and S. Borrmann (2009), Riming of graupel: Wind tunnel investigations of collection kernels and growth regimes, *J. Atmos. Sci.*, *66*, 2359–2366, doi:10.1175/2009JAS2969.1.

Waliser, D. E., et al. (2009), Cloud ice: A climate model challenge with signs and expectations of progress, *J. Geophys. Res.*, *114*, D00A21, doi:10.1029/2008JD010015.

Wang, L.-P., O. Ayala, S. E. Kasprzak, and W. W. Grabowski (2005), Theoretical formulation of collision rate and collision efficiency of hydrodynamically interacting cloud droplets in turbulent atmosphere, *J. Atmos. Sci.*, *62*, 2433–2450, doi:10.1175/JAS3492.1.

Westbrook, C. D., R. J. Hogan, and A. J. Illingworth (2008), The capacitance of pristine ice crystals and aggregate snowflakes, *J. Atmos. Sci.*, *65*, 206–219, doi:10.1175/2007JAS2315.1.

Yin, Y., K. S. Carslaw, and G. Feingold (2005), Vertical transport and processing of aerosols in a mixed-phase convective cloud and the feedback on cloud development, *Q. J. R. Meteorol. Soc.*, *131*, 221–245, doi:10.1256/qj.03.186.